POLITECNICO
MILANO 1863

SCUOLA DI INGEGNERIA INDUSTRIALE
E DELL'INFORMAZIONE

Role of Predictive Control and Risk-Aware Optimization in the Long-Term Design of a Green Microgrid under Renewable Uncertainty

Tesi di Laurea Magistrale in
Energy Engineering - Ingegneria Energetica

Author: **Federico Mattiuz**

Student ID: 247351
Advisor: Prof. Giampaolo Manzolini
Academic Year: 2024-25

Abstract

This work investigates the role of predictive control in the economic planning of a green microgrid by embedding a Model Predictive Control (MPC) algorithm within a lifetime simulation for the optimal design of the system. Results show that the economic value of storage depends on the control strategy when the system is sufficiently covered by the grid. Moreover, operational flexibility largely affects the optimal long-term design of the system, reducing the need for structural reinforcement. Predictive control also manages effectively uncertainty on photovoltaic production, without the need of additional risk-averse formulations.

Keywords: Optimization, Predictive Control, Uncertainty, Renewable Microgrid.

Abstract (IT)

Questo lavoro indaga il ruolo del controllo predittivo nella pianificazione economica di una microrete con energia rinnovabile, utilizzando un algoritmo di smart-charging all'interno di una simulazione per il dimensionamento ottimale del sistema considerato. I risultati mostrano che il valore economico della batteria dipende dalla strategia di controllo quando il sistema è sufficientemente coperto dalla rete elettrica. Inoltre, la flessibilità operativa influenza notevolmente la prestazione a lungo termine, riducendo la necessità di aumentare la complessità del sistema. Il controllo predittivo gestisce efficacemente anche l'incertezza nella produzione fotovoltaica, senza la necessità di introdurre formulazioni aggiuntive per quantificare il rischio che ne deriva.

Parole chiave: Ottimizzazione, Controllo predittivo, Incertezza, Microrete rinnovabile.

Contents

Abbreviations

EV	Electric Vehicles
PV	Photovoltaic
NPC	Net Present Cost
GWP	Global Warming Potential
FLB	First Life Batteries
SLB	Second Life Batteries
MPC	Model Predictive Control
MILP	Mixed Integer Linear Problem
SOH	State of Health
SOC	State of Charge
HSD	Homogeneous Self Dual
CVaR	Conditional Value at Risk

1 | Introduction

The diffusion of electric vehicles (EV) to reach climate and sustainability targets requires the deployment of a growing number of charging stations, creating a problem of energy management: since EV could represent a significant share in the transport sector, in the next years their presence as a load on the electrical grid could create unpredictable voltage and frequency variations [5] and require significant investments dedicated to the reinforcement of the infrastructure.
An efficient control strategy at different levels is required to face these issues. Studies such as [11] highlight the potential of EV batteries to provide flexibility to shift the charging process and improve grid stability or decrease costs and emissions. To do this, software-controlled charging could be key factor for efficient load distribution. Other studies such as [6] show that EV can also share their power with the grid or other loads, and be actively involved in power exchange stabilization. Again, smart control systems play a key role in energy management.
Another fundamental aspect of research for this topic is renewable integration. The variability of renewable energy generation extends the purpose of smart energy management beyond the interaction with the grid, creating an opportunity to further reduce costs and emissions by exploiting renewable energy in an efficient way. Charging stations equipped with photovoltaic (PV) panels and batteries may reach a good level of autonomy from the grid and reduce power grid reinforcement, as well as improve stability and reduce the need of investments. Of course, the installation of those components represent additional costs and externalities, which are correlated to their size, as well as the potential renewable share that is achieved. This tradeoff needs to be addressed when searching for an optimal configuration at system level, depending on its features and application. To account for this, the work presented in [2] develops an algorithm to search for the optimal configuration of such systems from the perspective of long-term economic planning. The study focuses on a design approach to minimize the Net Present Cost (NPC) and the Global Warming Potential (GWP) when performing an optimal dispatch. In particular, the impact of the use of First Life Batteries (FLB) and of Second Life Batteries (SLB) is assessed. Results showed that FLB are not considered as part of the optimal solution

because of their higher costs and emissions, while SLB show instead an optimal size for application because of their lower costs and emissions, increasing even more the income of the system and the satisfaction of the EV charging demand. Future improvements considered the implementation of uncertainties of renewable generation and consequently to increase the robustness of the optimization model.

The unpredictability of renewable energy generation can impact the optimal energy management and represent an issue for efficient EV charging, even with an optimal sizing of PV and battery. This is why predictive optimization models are needed: the possibility to create a realistic prediction of the future power generation and to operate in real time correcting forecast errors is of key importance to reach an optimal management of the system. In [1], a two-layer predictive control algorithm is presented for a green microgrid for EV charging. The study focuses on the inherent flexibility coming from the EV batteries during the charging process, which can be shifted in time to better match renewable generation and changing electricity prices, while minimizing power draw from the grid. Results confirm that the algorithm performs better than conventional dynamic programming algorithms that often require user inputs such as departure time, further improving the degree of automation of the system.

In this work, the objective is to evaluate the effect that predictive control could have on the optimal long-term design. The predictive control algorithm used in [1] is integrated in an economic simulation of the system considered in [2] and then used as a benchmark for a risk-aware stochastic Model Predictive Control (MPC) algorithm. The purpose is to continue the future work intended in [2], considering the use of SLB as an improvement in the economic planning of the system and to adopt predictive control as an effective way to deal with renewable generation uncertainties. The present work, together with [1] and [2], was carried out in the framework of the I-REVE project, supported by the "Investment Program for the Future" operated by ADEME, the French Environment and Energy Management Agency.

2 | Methodology

2.1. Description of Initial Models and Related Assumptions

2.1.1. The optimization model for long-term design

The model in [2] employs a single-objective economic Mixed Integer Linear Problem (MILP) optimization to solve a simulation of the system operation on a weekly time horizon, with a time step of one hour. The optimization is repeated for every week of the system lifetime, assumed of 24 years. Multiple simulations with different sizes of PV and battery create a screening from which a Pareto front evaluated on costs and emissions is found. The detailed structure of the MILP model is reported in Appendix A.2. At the end of each week, the degradation of the battery is assessed by computing the capacity loss via a State of Health (SOH) curve obtained from manufacturer data. Loads from the EV follow a fixed profile, which is defined for every week by dividing equally the total energy required by the vehicles at the charging station for their time of staying. The PV production is perfectly known. A typical year of PV data is repeated for every year of simulation, with each optimization considering the corresponding week. The objective of the simulation is to minimize the NPC of the system, which is actualized every year with a fixed discount rate.

2.1.2. The predictive optimization model for online energy management

The second model in [1] is a two-layer MPC optimization algorithm that simulates the system performance for a day of operation, with a time step of ten minutes. The controller finds the optimal decision set with a shrinking time horizon approach: the optimization problem is solved at every time step, with the end of the time horizon fixed. Each decision variable is an array of values, the first of which represents the controller decision for the current time step and the following ones are the prediction for the remaining part of the time horizon. A detailed description of this kind of predictive control is given in [7] for the same case study. The objective function minimizes power draw from the grid, while satisfying the load demand. Degradation of the battery is not considered since the time horizon is restricted, and the battery is assumed to operate without losses. To simulate uncertainties of PV production, an average profile is defined from a reference month, leaving to the lower layer the task to adapt to the real power generated. The load from the charging points is now a decision variable, bounded by the power profiles obtained in the cases of recharging at maximum power at the first or at the last moment available (Figure 2.1). The formulation of the MPC model can be found in Appendix A.1.

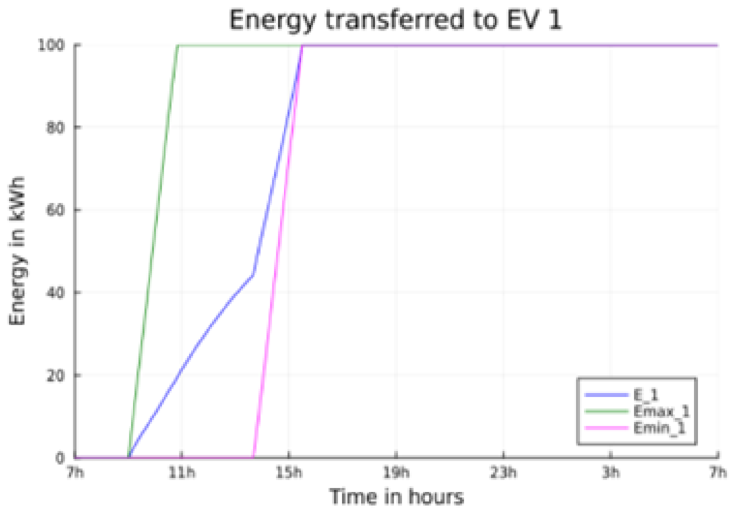

Figure 2.1: Profile obtained for the electric power used for recharging a bus. The two bounding profiles are given by the two possible control strategies that limit the domain of operation of each charging station.

2.2. Definition of MPC for the Optimal Design Simulation

The MPC model was modified to substitute the MILP model in the lifetime simulation. The first concern was to reduce computational time as much as possible, as the multiple iterations required for the same time horizon make a predictive model more time-demanding, especially when simulating on the entire lifetime of the system. Moreover, a predictive control update time is usually fast enough to respond rapidly to uncertainties. Increasing the time step to one hour allowed to obtain a significant reduction in computational time, because of the reduced dimensions of the problem and also because of the lower number of times the optimization had to be performed, as both depend from the

resolution of the model on the time horizon. No significant changes in demand satisfaction or self production were observed when increasing the time step. The results of this test are available in Appendix B.1.
Two different MPC models were compared for computational time required and robustness against uncertainties on the time schedule of the buses, namely a shrinking time horizon MPC and a rolling time horizon MPC. The first outperformed the second in both tests, proving that it was the best option. For a shrinking time horizon MPC in fact, each optimization is faster because the problem dimensions decrease at every iteration. Also, when facing uncertainties, the fixed end of the time horizon allows to better correct the trajectory of the decision variables. A comparison for the two tests is presented in Appendix B.2.
Finally, the solver for the model was selected as an Homogeneous Self Dual (HSD) Method, an interior-point method that allows to obtain smoother profiles of the decision variables, as it searches for optimal solutions far from boundaries [12], resulting in less fluctuations of the power flowing in and out of the components and consequently in less degradation. A comparison of the two solvers managing the energy in the battery is given in Appendix B.3.

2.2.1. Assumptions for the integration

The economic and structural assumptions for the algorithm resulting from the integration of the predictive control in the lifetime simulation of the system are the same as the algorithm described in Section 2.1.1. Everything that concerns the system operation from a long-term perspective is defined by the same algorithm, meaning that the actualization of the NPC, the update of battery SOH and the PV generation data are considered the same.
When considering the part related to the energy management of the system, which is mainly represented by the definition of the optimization problem, the new algorithm keeps the assumptions described in Section 2.1.2. In particular, the load will become a decision variable bounded as in Fig. 2.1, since the control is now predictive.
Some adaptations were carried out for a meaningful comparison with the MILP model. First, the power of the auxiliary components P_r, modeled as an electrical resistance, had to be assumed equal to zero when evaluating the impact of the predictive logic in the simulation, as it represents a constant load that equally penalizes every configuration. Additionally, it was assumed that the MPC model could consider the real PV profile in the prediction horizon of the optimization problem. Uncertainties for the future PV generation were modeled after the comparison between the two models.

2.2.2. Structure of the MPC Model for the Lifetime Simulation

The main decision variables, which for every time step are the total power to the vehicles $P^*_{EV}(t)$, the power exchanged with the battery $P^*_{bat}(t)$, the PV power generated $P^*_{PV}(t)$ and the slack energy of shedding $\varepsilon^*(t)$ are grouped as follows:

$$x(t) = \begin{pmatrix} P^*_{EV}(t) \\ \vdots \\ P^*_{EV}(t_f) \\ P^*_{bat}(t) \\ \vdots \\ P^*_{bat}(t_f) \\ P^*_{PV}(t) \\ \vdots \\ P^*_{PV}(t_f) \\ \varepsilon^*_1 \\ \vdots \\ \varepsilon^*_{t_f} \end{pmatrix} \in \mathbb{R}^{4n(t)}. \tag{2.1}$$

Alongside with the decision variables for the power exchanged with the grid, together with their bounds:

$$\mathbf{0}_{n(t)\times 1} \leq (P^*_{grid,IN}(t))_{t=1}^{t_f-1} \leq P_{grid,MAX}\,\mathbf{1}_{n(t)\times 1} \tag{2.2a}$$

$$\mathbf{0}_{n(t)\times 1} \leq (P^*_{grid,OUT}(t))_{t=1}^{t_f-1} \leq P_{grid,MAX}\,\mathbf{1}_{n(t)\times 1} \tag{2.2b}$$

The decision vector (2.1) requires the following bounds:

$$ub = \begin{pmatrix} P_{EV,max}\,\mathbf{1}_{n(t)\times 1} \\ P_{bat,max}\,\mathbf{1}_{n(t)\times 1} \\ P_{PV,prediction}(t) \\ \vdots \\ P_{PV,prediction}(t_f-1) \\ \hat{\varepsilon}\,\mathbf{1}_{n(t)\times 1} \end{pmatrix} \tag{2.3a}$$

$$lb = \begin{pmatrix} \mathbf{0}_{n(t)\times 1} \\ -P_{bat,max}\,\mathbf{1}_{n(t)\times 1} \\ \mathbf{0}_{n(t)\times 1} \\ \mathbf{0}_{n(t)\times 1} \end{pmatrix} \tag{2.3b}$$

Where an arbitrary constant $\hat{\varepsilon}$ is placed in (2.3a) to limit ε_t^*. $P_{pv,prediction,t}$ is the upper bound of the decision variable $P_{pv,t}^*$. This gives the controller the freedom to apply a curtailment if necessary. However, it will be encouraged to use as much as photovoltaic power as possible by the objective function itself, passing through the following constraint that expresses the energy balance of the system:

$$P_{grid,in}^*(t) - P_{grid,out}^*(t) - P_{EV}^*(t) + P_{bat}^*(t) + P_{PV}^*(t) - P_r = 0 \qquad t = 1, 2, \ldots, t_f. \tag{2.4}$$

The energy inside the battery w_t^* is considered as a state variable, in the same way as $E_{EV,t}$ is considered in Equations (A.7) and (A.8):

$$\begin{cases} -P_{bat,t}^* \cdot \Delta t \leq \mathcal{W}_{t+1}^{max} - w_t \\ -P_{bat,t}^* \cdot \Delta t - P_{bat,t+1}^* \cdot \Delta t \leq \mathcal{W}_{t+2}^{max} - w_t \\ \vdots \\ -P_{bat,t}^* \cdot \Delta t - P_{bat,t+1}^* \cdot \Delta t - \cdots - P_{bat,t_f-1}^* \leq \mathcal{W}_{t_f}^{max} - w_t \end{cases} \tag{2.5a}$$

$$\begin{cases} P_{bat,t}^* \cdot \Delta t \leq w_t - \mathcal{W}_{t+1}^{min} \\ P_{bat,t}^* \cdot \Delta t + P_{bat,t+1}^* \cdot \Delta t \leq w_t - \mathcal{W}_{t+2}^{min} \\ \vdots \\ P_{bat,t}^* \cdot \Delta t + P_{bat,t+1}^* \cdot \Delta t + \cdots + P_{bat,t_f-1}^* \leq w_t - \mathcal{W}_{t_f}^{min} \end{cases} \tag{2.5b}$$

This gives the controller more freedom and stability as there is just one bound on w_t^* expressed by (2.5), whereas before Eq. (A.12) and (A.2) were applying constraints on the same decision variable. The slack variable for shedding was introduced in Eq. (2.7), while

Eq. (2.6) was left unchanged from the original MPC version.

$$\begin{cases} P^*_{EV,t} \cdot \Delta t \leq E^{max}_{t+1} - E_{EV,t} \\ P^*_{EV,t} \cdot \Delta t + P^*_{EV,t+1} \cdot \Delta t \leq E^{max}_{t+2} - E_{EV,t} \\ \vdots \\ P^*_{EV,t} \cdot \Delta t + P^*_{EV,t+1} \cdot \Delta t + \cdots + P^*_{EV,t_f-1} \cdot \Delta t \leq E^{max}_{t_f} - E_{EV,t} \end{cases} \tag{2.6}$$

$$\begin{cases} -P^*_{EV,t} \cdot \Delta t - \varepsilon^*_k \leq E_{EV,t} - E^{min}_{t+1} \\ -P^*_{EV,t} \cdot \Delta t - P^*_{EV,t+1} \cdot \Delta t - \varepsilon^*_{t+1} \leq E_{EV,t} - E^{min}_{t+2} \\ \vdots \\ -P^*_{EV,t} \cdot \Delta t - P^*_{EV,t+1} \cdot \Delta t - \cdots - P^*_{EV,t_f-1} \cdot \Delta t - \varepsilon^*_{t_f-1} \leq E_{EV,t} - E^{min}_{t_f} \end{cases} \tag{2.7}$$

The objective function was changed to be the same as the one used in the MILP model:

$$\begin{split} \min \sum_{t=1}^{t_f-1} \big(C_{grid,in}(t) \cdot P^*_{grid,in}(t) - C_{grid,out} \cdot P^*_{grid,out}(t) - C_{EV} \cdot P^*_{EV}(t)\big) \cdot \Delta t \\ + \sum_{t=1}^{t_f-1} C_{EV} \cdot \varepsilon(t) \end{split} \tag{2.8}$$

This implies that now the cost of operation is minimized, instead of the power taken from the grid. The algorithm has a post-optimization control logic that defines the real value of every decision variable during the online operation, to respect the physical limits of the system. A block diagram of the procedure adopted is in Appendix A.3. Priority is given to exploit all available energy from the PV panels, and curtailment activates only if selling energy to the grid has reached the maximum power allowed.

2.3. Characterization of the Predictive Control

2.3.1. Further Developments

A further characterization of the MPC model after the comparison with the MILP optimization was made to assess its applicability in real cases. Uncertainties on the photovoltaic production were introduced and the optimization problem modified to consider multiple scenarios depending on the probabilistic distribution of solar irradiance. A risk assessment function was embedded in the objective function to make the model aware of the unpredictability of renewable generation.

Uncertainties were modeled starting from a set of 16 years of historic data on solar irradiance from the location of interest, which was processed to obtain a typical day for each month of the year. As a physical phenomena, the solar irradiance for a set of data at a defined time produces a bimodal distribution, since most of the values correspond either to clear sky or night time, with intermediate values representing cloudy days. Therefore, the probability distribution can be represented by a Beta distribution [9].
The objective function considers a risk-awareness function to avoid the possibility of incurring in higher costs of operation because of unexpected deficit in the PV generation. To this purpose, the Conditional Value at Risk (CVaR) function described in [8] is an intuitive and straight-forward function for risk assessment in stochastic models [10].
The decision output for the lower layer in charge of simulating the online energy management of the system was selected as the worst case scenario. This approach is followed from [14] to ensure a conservative approach when mitigation of adverse scenarios is a priority.

2.3.2. Integration of the Battery Efficiency in the Optimization

The model can consider battery losses during charge and discharge instead of leaving the control to adapt. When moving to a more realistic formulation of the MPC model, the set of constraints for the exchange of energy with the battery were modified as follows:

$$\begin{cases} -\eta \cdot P^*_{bat,t} \cdot \Delta t \leq \mathcal{W}^{max}_{t+1} - w_t \\ -\eta \cdot P^*_{bat,t} \cdot \Delta t - \eta \cdot P^*_{bat,t+1} \cdot \Delta t \leq \mathcal{W}^{max}_{t+2} - w_t \\ \vdots \\ -\eta \cdot P^*_{bat,t} \cdot \Delta t - \eta \cdot P^*_{bat,t+1} \cdot \Delta t - \cdots - \eta \cdot P^*_{bat,t_f-1} \leq \mathcal{W}^{max}_{t_f} - w_t \end{cases} \tag{2.9a}$$

$$\begin{cases} \frac{P^*_{bat,t}}{\eta} \cdot \Delta t \leq w_t - \mathcal{W}^{min}_{t+1} \\ \frac{P^*_{bat,t}}{\eta} \cdot \Delta t + \frac{P^*_{bat,t+1}}{\eta} \cdot \Delta t \leq w_t - \mathcal{W}^{min}_{t+2} \\ \vdots \\ \frac{P^*_{bat,t}}{\eta} \cdot \Delta t + \frac{P^*_{bat,t+1}}{\eta} \cdot \Delta t + \cdots + \frac{P^*_{bat,t_f-1}}{\eta} \leq w_t - \mathcal{W}^{min}_{t_f} \end{cases} \tag{2.9b}$$

According to [3], considering battery efficiency only post-optimization can lead to an increase in losses. In fact, since efficiency itself is not optimized, the control will be exposed to a sub-optimal operation. This can be an approach to test the robustness of the model when reacting to an unpredicted bias affecting the state of the system, but it also introduces a virtual penalization on the battery that could make its use unjustified. If the battery is considered ideal, and its losses are modeled as a mismatch between the value defined by the model and the one managed by the controller, the grid has to cover for the remaining power. This can be meaningful for control purposes, as the grid acts to compensate for the unpredicted battery loss, and it can be representative of the system real behavior from an online grid management perspective. However, from a long-term design perspective this introduces an additional cost related to the use of the battery, penalizing its contribution. To account for this, the loss in the battery were considered at his side and not at the control node:

$$w_{t+1} = w_t - \frac{P_{bat,t} \cdot \Delta t}{\eta} \qquad (\text{Discharge}, P_{bat,t} > 0) \tag{2.10a}$$

$$w_{t+1} = w_t - P_{bat,t} \cdot \Delta t \cdot \eta \qquad (\text{Charge}, P_{bat,t} < 0) \tag{2.10b}$$

In this way, $P_{bat}(t)$ at control level is what the model predicted. Together with the efficiency considered inside the optimization, the battery is not penalized from the point of view of the lifetime performance.

2.3.3. Stochastic Modeling of Uncertainties on the PV Production

A predictive model should consider uncertainties on future data, such as the photovoltaic production. This was accounted for in [7] by considering an average profile on a reference week. Seasonal variation was created by averaging on different months from a set of yearly data. This approach is acceptable as a baseline when considering uncertainties. However, uncertainties are usually modeled starting from a distribution of historical data, to create a stochastic representation of the unpredictability of renewable generation. A Beta distribution function is used as in [4] for solar irradiance:

$$f_{P_{\mathrm{PV}}}(p \mid i, t) = \frac{1}{\mathrm{B}(\alpha_{i,t}, \beta_{i,t})} \, p^{\alpha_{i,t}-1} \, (1-p)^{\beta_{i,t}-1}, \qquad 0 \le p \le 1 \tag{2.11}$$

$$\alpha = \begin{cases} 0.1, & k \leq 0 \\ \mu\, k, & k > 0 \end{cases} \qquad \beta = \begin{cases} 100, & k \leq 0 \\ (1-\mu)\, k, & k > 0 \end{cases} \qquad \text{with:} \qquad k = \frac{\mu(1-\mu)}{\sigma} - 1 \quad (2.12)$$

Where $\alpha = 0.1$ and $\beta = 100$ correspond to a flat Beta distribution, to account for the absence of solar irradiation during night. Seasonal variation was considered by grouping together historical data per month. Each distribution was created normalizing the historical data to the maximum value of power $P_{max}(i,t)$. During the simulation, the parameters $\alpha(i,t)$ and $\beta(i,t)$ along with $P_{max}(i,t)$ define the probabilistic PV distribution at every future time step:

$$P_{PV}(i,t) = PV_{installed} \cdot \eta_{inv} \cdot \tilde{p}(i,t) \cdot P_{max}(i,t) \quad (2.13)$$

2.3.4. Implementing Risk-Awareness with CVaR

The objective function must include a risk function to make the model aware of potential losses deriving from low irradiance scenarios. In this way, the model can select a more conservative approach, ensuring energy availability. To do this, The CVaR function was adopted, following its definition by Rockafellar and Uryasev in [8], and it was integrated as [10] and [13].

$$\mathrm{CVaR}_\epsilon(C(i)) = \eta + \frac{1}{(1-\epsilon)N_s}\sum_{i=1}^{N_s} \max(C(i)) - \eta,\, 0) \quad (2.14)$$

With η being the Value at Risk VaR_ϵ of the worst scenarios represented by the tail of the distribution beyond the threshold ϵ. Considering 30 different scenarios (a larger number would have excessively increased the computational time), it is advisable to keep $\epsilon = 0.8$. The use of $CVaR_\epsilon$ allows to weight the average cost of the worst scenarios. The objective function is defined as follows:

$$\min\, (1-\lambda)\,\mathbb{E}[C(i)] + \lambda\,\mathrm{CVaR}_\epsilon(C(i)) \qquad i = 1, \ldots, N_s \quad (2.15)$$

Where $C(i)$ is calculated as in Eq. (2.8) and λ is the weight of risk awareness. Once a set of costs is obtained, the worst case scenario in terms of higher costs is selected to maintain a conservative approach, thus ensuring enough energy availability during online

energy management.
To evaluate the effect of the CVaR function, an alternative version of the MPC model was created considering a PV profile defined as the median of the Beta distribution at every time step (Eq. (2.16)). A median profile can be considered as a good approximation of the real PV generation, leaving the correction of forecast errors to the lower layer of the controller.

$$p_{\mathrm{MP}}(t) = \mathrm{median}[\mathrm{Beta}(\alpha_t, \beta_t)]\,, \qquad t = 1, \ldots, T \tag{2.16}$$

3 | Case Study

The models presented in Chapter 2, the ones used in the previous related works and in this present work, consider the same case study which is described in the following. The model built for the simulation considers the structural features of the demonstration prototype of a charging station constructed by the companies involved in the I-REVE project. The prototype is located in a rural region of France, where it can be assumed that the grid infrastructure could need reinforcement if a new charging station is constructed, allowing to simulate the operation for a realistic scenario under the assumptions initially made on the convenience of renewable integration on EV charging stations.

The system can be modeled as a single node DC microgrid (Appendix A.4). It is assumed that the system will operate for 24 years. The battery and the grid can exchange power in both directions, while the PV acts as a generator and the EV chargers as a load. The sign convention assumes positive sign for the power entering the central node, which represents the controller, and negative sign for the power going towards the components. The power limit is defined for each branch.

The technical features that characterize the microgrid are completely described in [2]. The grid allows an exchange of power up to the limit of 36 kW. Purchasing energy follows a cost schedule that changes from 0.214 €/kWh during day to 0.136 €/kWh at night, while selling is fixed at 0.078 €/kWh. The tariff for recharging is assumed to be 0.389 €/kWh. The battery power limit is fixed at 40 kW and its capacity is a design variable. The PV peak power is also a design variable. PV and battery are characterized by specific costs and emissions per unit of kWp and kWh installed. Concerning the battery, the use of SLB is modeled by assuming that its use starts with 90% of the design capacity, and its specific costs and emissions are reduced to around one third of the values for FLB.

The power to the EV charging points can be defined by a fixed load profile or can be bounded and become a decision variable (Fig. 2.1), depending on the model chosen. Five buses with a battery capacity of 100 kWh represent the load. When considering operation with a predictive control, the time schedule of the buses is assumed to be defined and constant for every simulated day. Three charging points are available, one with a maximum power of 50 kW, and two with a maximum power of 22 kW.

4 | Results

4.1. Screenings for the Optimal Long-Term Design

This section presents the results obtained with different model structures, eventually introducing the assumptions to quantify their effect. A comparison of the optimal Pareto fronts obtained is given in the following section. Appendix C.1 contains figures useful to visualize the position of the Pareto fronts in the design search space obtained for each model.

4.1.1. MILP Screening with a weekly time horizon

A screening using the MILP model using a week long time horizon was performed, giving the results in Fig. 4.1. The optimal configurations are close to what was found in [2] for the SLB case. The only difference in the model formulation is constituted by the loads, which in [2] include 8 additional EVs.

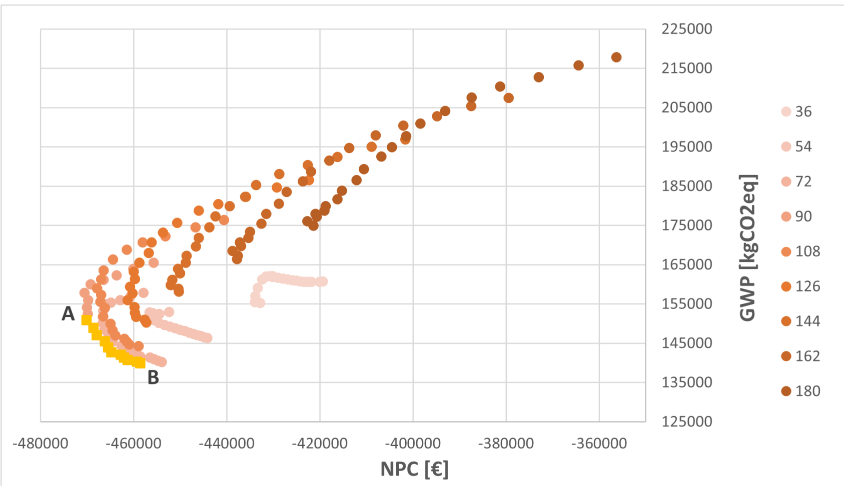

Figure 4.1: Economic-environmental evaluation of the screening results. The Pareto front (A-B) is identified. Each point corresponds to a single lifetime simulation. The color gradient represents the PV power in kW.

4.1.2. MILP Screening with a daily time horizon

A new screening was performed using a version of the MILP algorithm with a daily time horizon, and a new Pareto curve was obtained as reported in Fig. 4.2. The curve C-D of configuration points is the one that will assess the effect of a predictive control on the optimal design, as this model is defined in the same framework of its MPC counterpart.

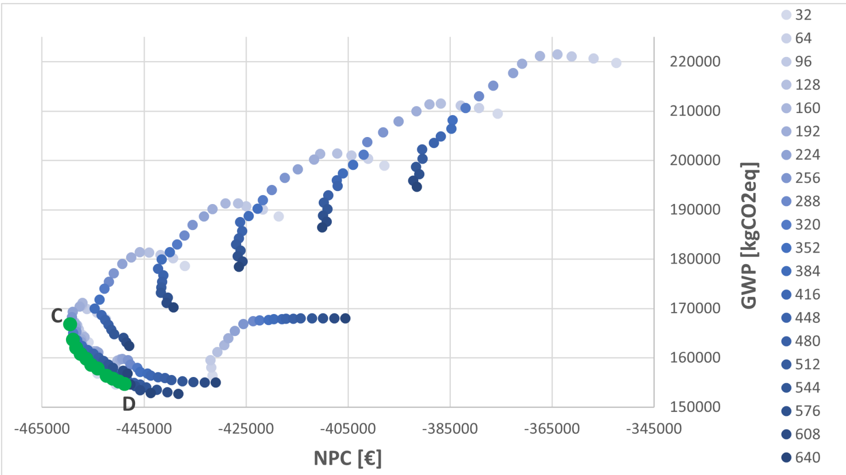

Figure 4.2: Screening obtained using the MILP algorithm with a time horizon of 24 hours. The color gradient indicates the initial battery capacity in kWh.

4.1.3. MPC Screening under compatible assumptions with the MILP model

The interest in having a predictive control integrated in a lifetime simulation is not only in seeing how it can improve the performance of a certain configuration, but also to see if, when performing a new screening, a new optimal front will be found with different configurations and a better performance than before.This could give a perspective on the link between predictive control and optimal design when comparing the results from both analyses.

The results obtained with a predictive control are presented in Fig. 4.3. The assumptions on the model features explained in subsection 2.2.1 were applied to isolate the effect of the predictive control on the optimal design. The Pareto curve is now formed by configurations for which the battery capacity is equal to zero, similarly to what was obtained for FLBs in [2].

This indicate that predictive control can provide enough operational flexibility to avoid the use of a storage when support from the grid is available. In this context, SLBs represent an avoidable cost. Differently from the FLB case in [2], where the absence of storage was attributed to its high costs of installation, here the determining factor is the adopted control strategy. This suggests that the system operation can influence the optimal design independently from economic assumptions, highlighting a modeling principle that may extend beyond the framework of this project.

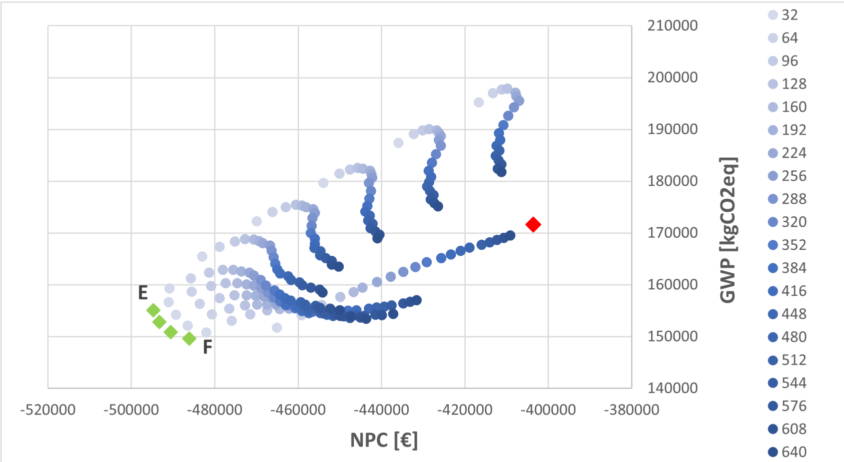

(a) Results grouped for different battery capacity. The color gradient stands for the initial battery capacity in kWh.

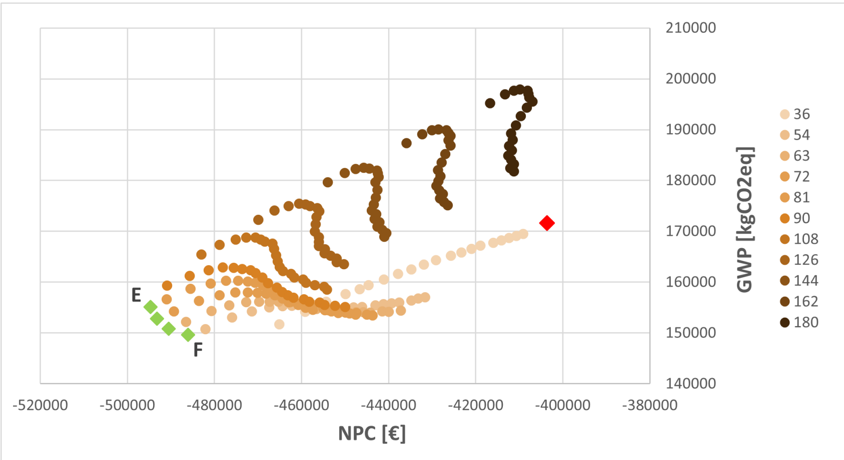

(b) Results grouped for different PV power installed. The color gradient stands for the peak PV power installed in kW.

Figure 4.3: Screening results for the MPC. The Pareto front is found with 0 kWh of battery capacity.

4.1.4. Assessment of the assumptions on the MPC

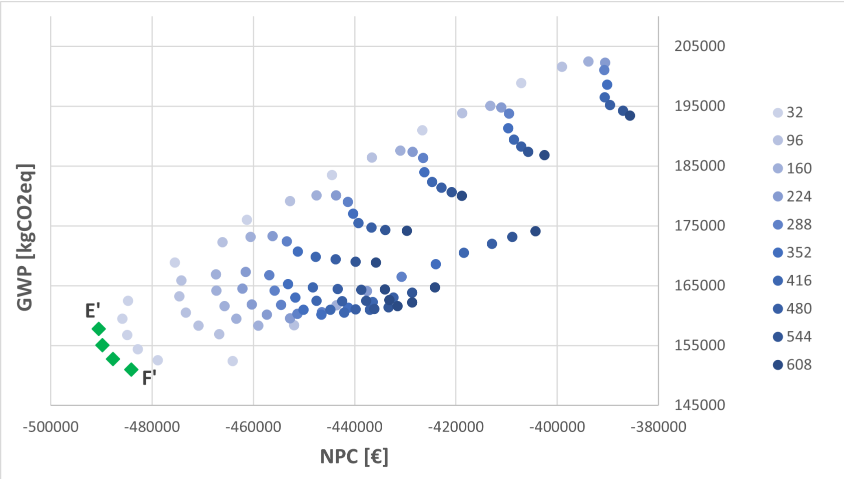

(a) The screening that generated the Pareto front E'-F' used an MPC with a prediction on the PV power.

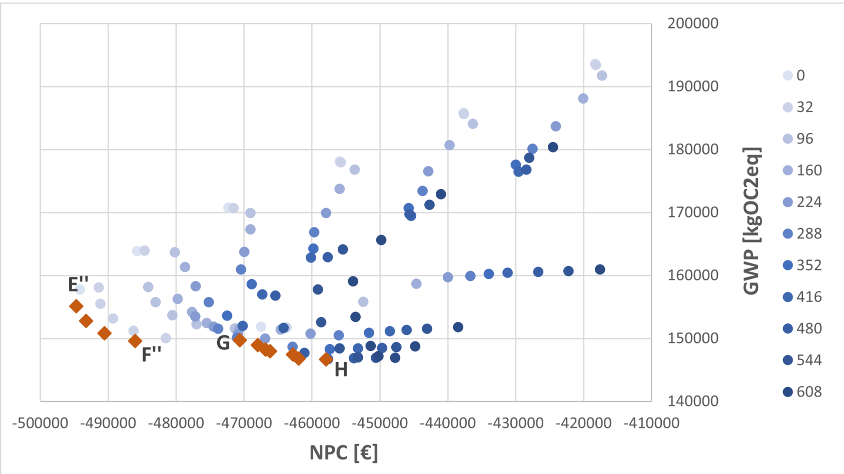

(b) Results obtained using an MPC considering a constant lower bound on the battery energy. The Pareto curve generated is divided in two groups. The part of the front G-H involves the use of a battery.

Figure 4.4: Results obtained to assess the impact of the assumptions made on the MPC. The color gradient stands for the initial battery capacity in kWh.

A simulation with uncertainties on the PV prediction as originally considered in [7] was performed to verify if the Pareto curve found above was a consequence of considering the PV profile to be perfectly known. As it is possible to see in Fig. 4.4a, this did not change the optimal configurations. In fact, without a stochastic model the optimization only produces a sub-optimal decision that is corrected afterwards.
A last screening was then performed to evaluate the effect of the constraint on the final State of Charge (SOC) $SOC(t_f) = 50\%$. The photovoltaic profile was again assumed

perfectly known. The screening reported in Fig. 4.4b produced a second group of non dominated points (G-H) which is characterized by the use of a battery. Despite their economic return not being as high as the points of the curve E"- F", the lower level of emissions make the configurations part of the optimal solution, suggesting that a more permissive use of the battery can make it emerge in the optimal configurations.

4.2. Comparison of Optimal Sets of Configurations

4.2.1. Effect of the assumptions on the MPC

The points in the curve E'-F' are dominated by the points of the curve E-F, suggesting that uncertainties on the PV production produce losses due to sub-optimal control. Moreover, the Pareto curve E"-F" is coincident with E-F. This is coherent since the model formulation is the same but with one constraint relaxed. The second group of optimal solutions (points G-H) suggest that the battery can be used less aggressively without imposing $SOC(t_f) = 50\%$, according to [3]. Using the screening obtained in Fig. 4.3 as a reference, Fig. 4.5 shows the relative position of the Pareto curves obtained with different MPCs.

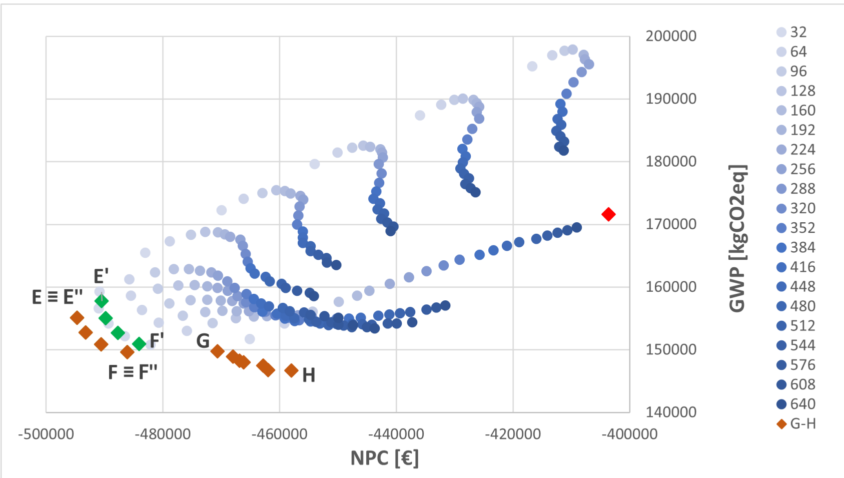

Figure 4.5: Position of the Pareto curves obtained using models with a prediction on the PV power (curve E'-F') and a relaxed constraint on the minimum SOC (curve E"-H). The assumptions preserve the optimal configurations found with an ideal MPC.

4.2.2. Change in the long-term design using different optimization models

A predictive control will preserve the optimal solutions or find additional ones, depending on the assumptions. When the structure of the model changes consistently, the set of

optimal solutions will change as well, along with their performance. This is what was observed when shifting from a MILP optimization to a predictive control. In Fig. 4.6a the Pareto curves obtained for different models are compared and their position in the design search space is shown in Fig. 4.6b.
The curve A-B is the result of a screening performed with a weekly time horizon MILP problem, and it dominates entirely the curve C-D, which was obtained with a daily time horizon MILP problem. This shows how much the performance of a model increases with the length of the time horizon considered in the optimization problem. Moreover, the optimal configurations in the search space will be similar. Curve C-D is then used as a benchmark for curve E-F, which is obtained with an MPC. The curve E-F dominates the curve C-D, suggesting that a predictive control is capable of finding a better set of solutions. Additionally, the optimal design will change significantly. All the curves dominate the grid-only configuration (without PV and battery installed), demonstrating the economic benefit deriving from the installation of green components.

Another way to characterize the effect of the predictive control is to evaluate how the optimal configurations will change when the MPC is applied. This is also done to verify the that the predictive control is properly defined, since adding another decision variable that was assumed constant (the energy demand from the buses) should let the optimization algorithm find a better solution for the system. For this purpose, the Pareto front determined by the optimal MILP model will be considered (i.e. the curve A-B in Fig. 4.1). The results in Fig. 4.6 show that a predictive control can improve the performance of a selected configuration: curve A1-B1 is dominated by A-B, indicating that shorter time horizon for the optimization will impact the system's operation, while curve A2-B2 dominates A1-B1 because of the use of the MPC, and A3-B3 shows a reduced level of emissions thanks to the increased availability of the battery.

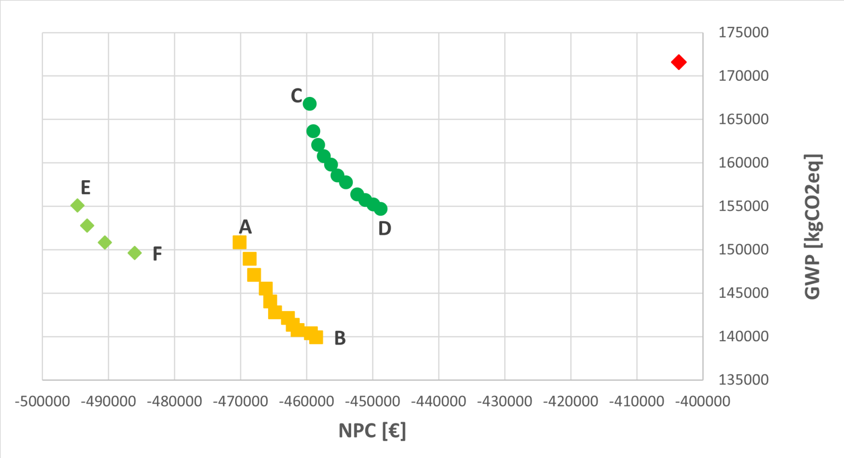

(a) Pareto curves obtained with different models. Curve A-B was obtained with a weekly time horizon MILP; curve C-D with a daily time horizon MILP; curve E-F with a daily time horizon MPC.

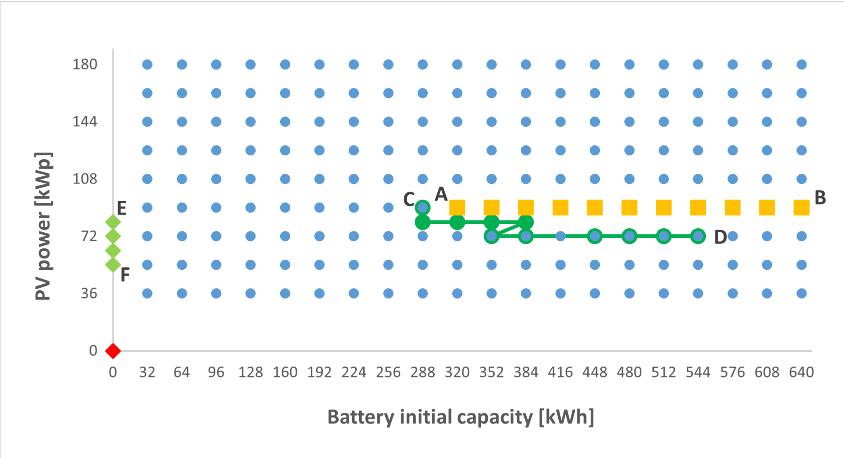

(b) Relative position of the Pareto curves in the design search space. The optimal design slightly differs when changing the time horizon of the MILP problem, whereas it varies greatly when using a predictive control.

These findings suggest a link between the energy management strategy and the economic planning of the system. In other words, the way in which a system is operated will greatly impact its value over time, and in particular the optimal design on the long term will be directly dependent from it. In the following section, the results obtained with a predictive control featuring the modifications mentioned in Section 2.3 are presented.

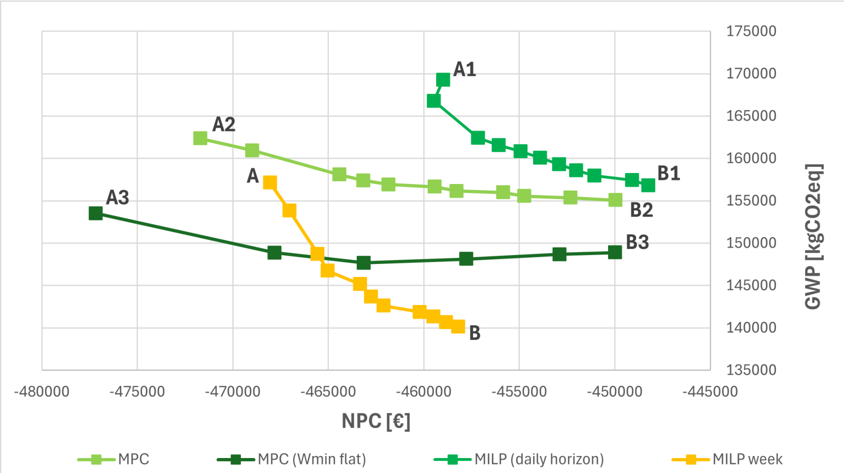

Figure 4.6: Relative position of the configurations of the original curve A-B when the simulation is carried out with different models. Curve A1-B1 is found with a daily time horizon MILP, curve A2-B2 with the MPC and curve A3-B3 by relaxing the constraint on the final SOC.

4.3. Role of Battery Efficiency and PV Uncertainties

4.3.1. Effect of the integration of the battery efficiency in the model

A screening with the MPC considering the battery efficiency is presented in Fig. 4.7. This modification to the problem structure allows the battery to emerge in the optimal configurations. However, the assumption of a perfectly known PV profile is still valid. Without uncertainties on the PV production, the control can use the battery without incurring in forecast errors, making it possible to exploit it in the most efficient way. For a realistic assessment of the predictive control operation, it is necessary to introduce uncertainties and verify if the battery maintains its competitiveness.

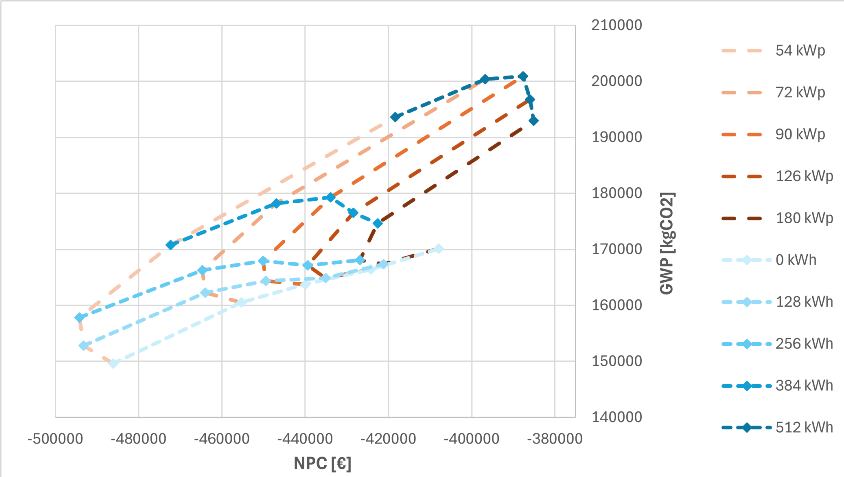

Figure 4.7: Screening obtained considering the battery efficiency as part of the optimization of the MPC. The Pareto front now considers the battery, but the assumption made on the PV profile could overestimate its value with respect to a realistic predictive control.

4.3.2. Introduction of uncertainties

With uncertainties on the PV profile, the controller input will have to be corrected post optimization, making the system unable to perfectly exploit the real production. Since the value of the battery mostly depends on how much photovoltaic energy is stored, it is not guaranteed that the storage will remain part of the optimal solution. Results for the MPC considering a median PV profile reported in Fig. 4.8 show that increasing the battery capacity decreases the performance of the system. A comparison using the stochastic model to simulate similar configurations (Fig. 4.9) shows that risk penalization increases costs on the lifetime, regardless the value of PV power installed. This is expected as the model is more conservative, according to [14], where it is indicated that economics and robustness are negatively correlated.

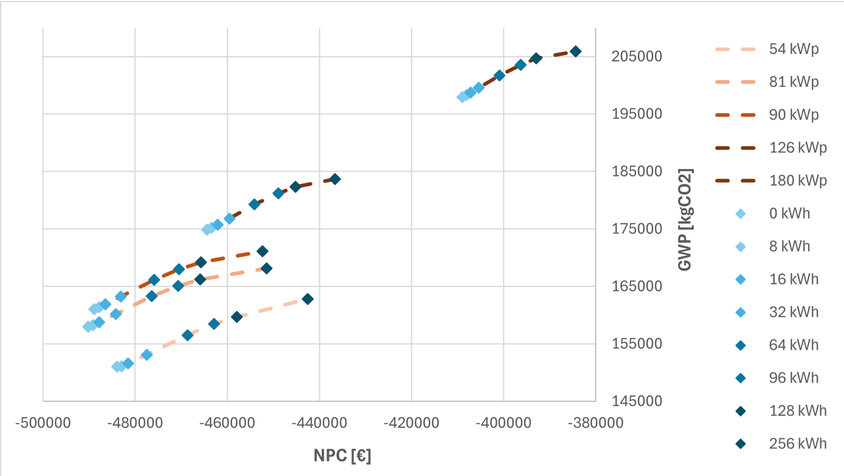

Figure 4.8: Screening performed with a predictive control and uncertainties on the PV production modeled as the median value for every time step.

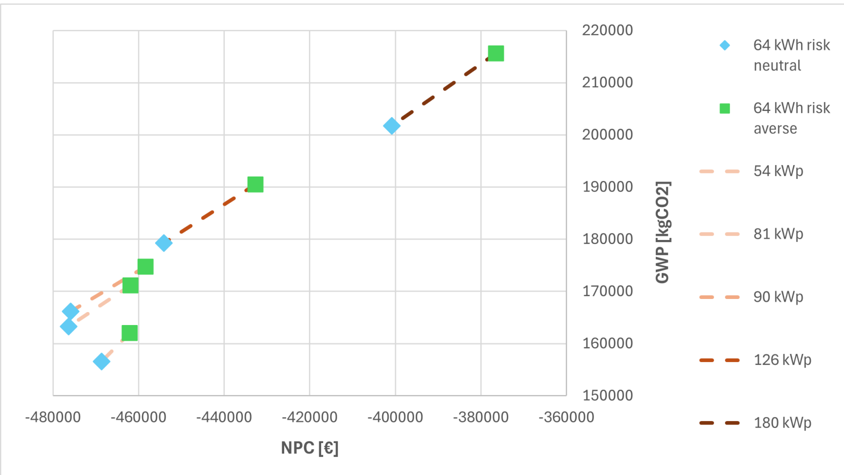

Figure 4.9: Comparison of the lifetime performance obtained for configurations considering uncertainties and different risk assessment. The green square represent the results obtained with a risk averse optimization.

5 | Discussion

5.1. Energy Flow Management and Battery Use in MILP and MPC Cases

The amount of energy stored inside the battery during summer and winter typical weeks represented in Fig. 5.1 and Fig. 5.2 show that, with a predictive control, the exchange of energy with the battery is reduced, resulting in less replacements during the lifetime (Fig. 5.3), with a consequent decrease in the installation costs.
At the same time, using a predictive control allows to manage the dispatch of energy to the buses, reducing the need of storing energy to better match the constant demand profile of the MILP case. The MPC will then improve the performance of configurations with smaller sizes of battery.

As Fig. 5.4 shows, a predictive control can supply more power when PV generation is high. Moreover, the constraint on the final state of charge becomes more demanding with the battery capacity, making high capacity storage more expensive during operation. This constraint was left as part of the optimization problem because it still represent an opportunity to perform night charging or prepare the battery to the uncertainties of the following day. Because of this, and the fact that buses stay overnight for charging, the operation will often saturates its intake from the grid during night. This represents an additional cost, but considering that the alternative is to oversize both the PV panels and the battery to provide and store enough energy to cover at least part of the night period, it is reasonable to assume that the grid can represent a more convenient alternative.

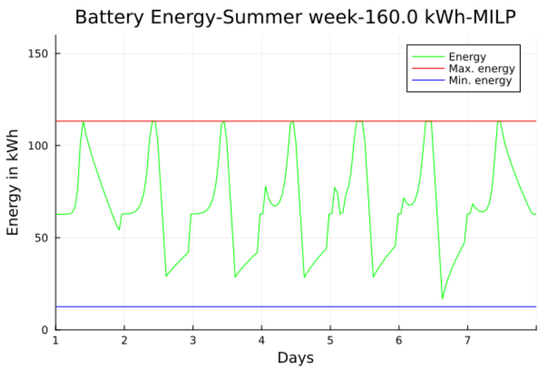

(a) Energy inside the battery on a typical week in summer with a MILP simulation. The constraint $SoC_{end} = 50\%$ is not visible as it is defined with the decision variable of the model, but it is present at the end of every day.

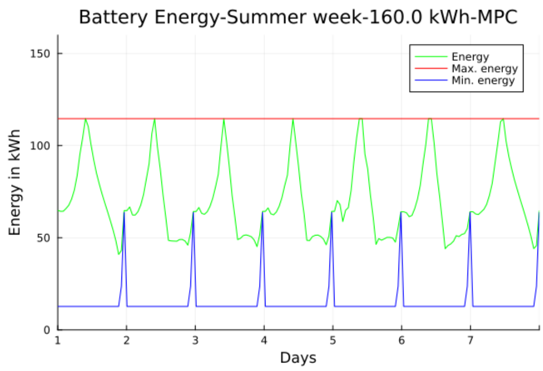

(b) Energy inside the battery on a typical week in summer with a MPC simulation. The blue line represent the lower constraint, going to the value corresponding to $SoC_{end} = 50\%$ at the end of each day.

Figure 5.1: Energy in a 160 kWh battery during a typical summer week simulated with MILP and MPC models. It is possible to see how the power exchange with a smart charging operation is more contained with respect to the previous model.

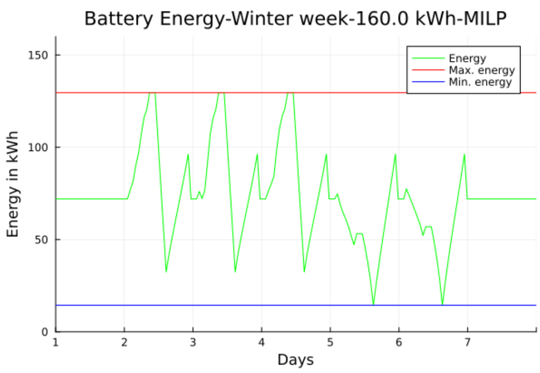

(a) Energy inside the battery on a typical week in winter with a MILP simulation.

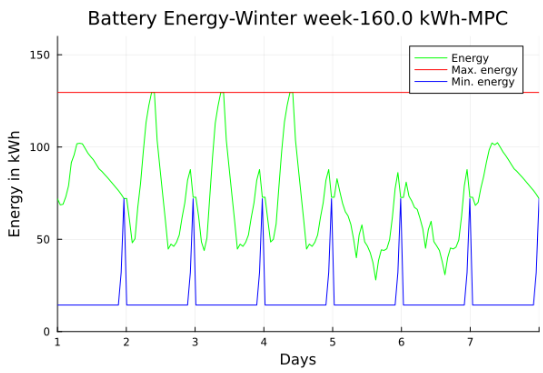

(b) Energy inside the battery on a typical week in winter with a MPC simulation.

Figure 5.2: Energy in a 160 kWh battery during a typical winter week simulated with MILP and MPC models. Even with a reduced use, resulting from the lower amount of PV power available, the MPC model discharges the battery in a more conservative way.

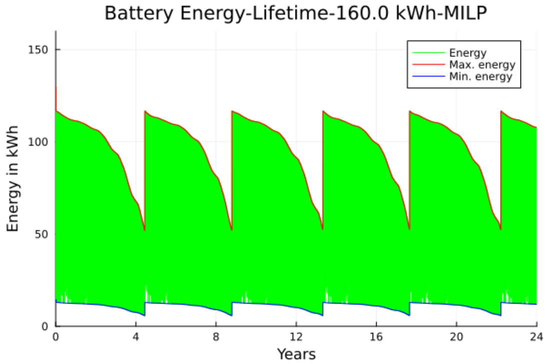

(a) Lifetime energy flow resulted from a MILP simulation.

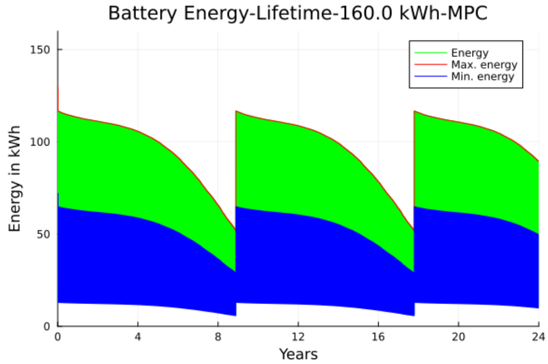

(b) Lifetime energy flow resulted from a MPC simulation.

Figure 5.3: Lifetime energy flow for a battery of 160 kWh obtained with a MILP and an MPC model. Each peak in the capacity corresponds to a replacement. It is possible to see that the number of replacements is lower for an MPC simulation, indicating a more conservative use.

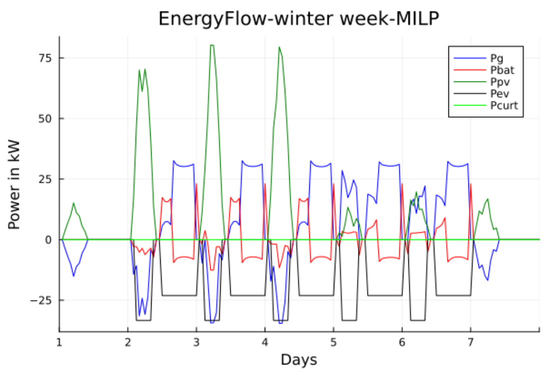

(a) Energy flow management for the MILP model.

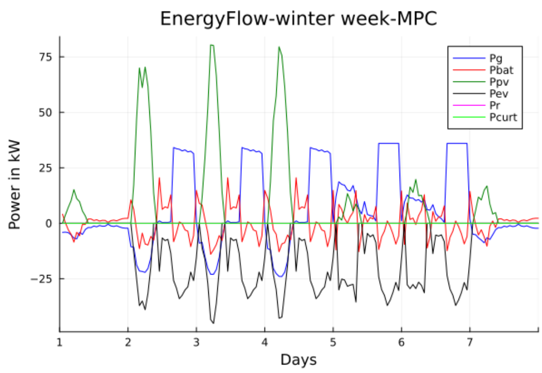

(b) Energy flow management for the MPC model.

Figure 5.4: Energy flow management on a reference winter week for MILP and MPC models.

5.2. Economic Assessment of the Battery

To evaluate the effect of the battery on costs, the components depending on the battery capacity (namely, operation costs and battery installation costs) that contribute to the lifetime Net Present Cost of the system where compared for different values of battery capacity.

Fig. 5.5a shows that, when considering two different levels of PV power installed, the specific costs of the battery are only dependent from its capacity, while the operation costs in Fig. 5.5b also depend on the size of PV, which allows to generate a higher amount of free energy and consequently improve revenues.

However, when comparing the trends at the highest level of PV considered a linear regression shows that the specific cost per kWh installed are higher than the specific revenues, bringing the costs of the battery to the winning side of a tradeoff between the two components. As a consequence, despite the battery will increase profits, from the long-term perspective it will also represent a significant investment, in particular because of multiple replacements caused by degradation.

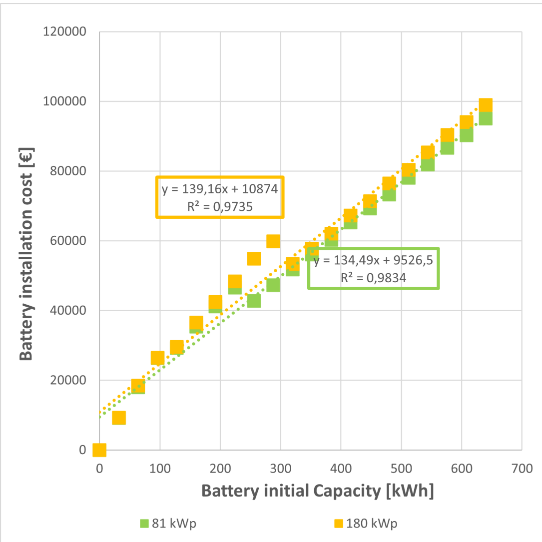

(a) Installation costs of the batteries of the solutions with 81 kWp and 180 kWp of PV power at different battery capacity. For both groups the specific cost is around 135 €/kWh.

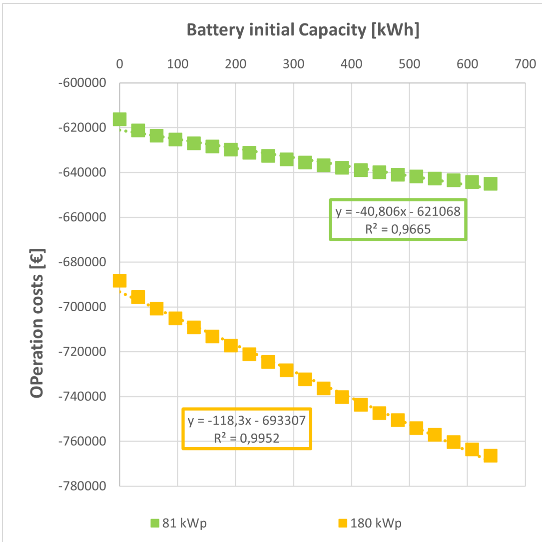

(b) Operation costs of the solutions with 81 kWp and 180 kWp of PV power at different battery capacity. In terms of revenues, at 180 kWp the operation grants about 120 € per kWh of battery installed, while at 81 kWp it drops to 40 €/kWh.

Figure 5.5: Plot of the two main terms that define the NPC. When reducing the PV power, the specific costs of operation increase due to the loss in the renewable share.

Considering that a predictive control can adopt smaller batteries and that an optimal range of PV peak power installed is already defined, it is possible to conclude that inside the lifetime framework of the system a smart charging algorithm can, in fact, produce optimal solutions without a battery, despite exceptional cases with strong assumptions on the model structure, such as not considering uncertainties on the renewable production.

5.3. Operation Performance and Risk Assessment

This section is dedicated to discuss the introduction of uncertainties and their impact on the system performance. Considerations on the stochastic nature of the PV profile and its requirements as a model input will be made, along with an evaluation of the seasonal variation for different configurations of the operation control and the risk-related values, drawing conclusions on the effect that uncertainties can have on the energy management. Finally, a tuning of the risk-aversion parameter will highlight key features related to the system robustness, revealing conceptual principles that affect its optimal design.

5.3.1. PV profile under uncertainties

When using a stochastic MPC it is necessary to evaluate in parallel a certain number of independent scenarios and optimize them at the same time. Despite the objective function considering all the scenarios combined, the optimization problem does not automatically select a scenario for the online operation. Instead, this will be selected from the model output following a logic defined *a priori*. In this case, considering the worst scenario allows to evaluate the effect of the CVaR function, since by reducing the tail of the cost distribution it would be expected a general improvement of the worst scenarios.

Fig. 5.6 shows a PV profile adopted post optimization by the online control selected as the worst case. Despite the reference week being in winter, the worst case distribution based on historical data can still be quite optimistic on the expected generation. This could exclude the selected scenario from the ones minimized by the CVaR, therefore reducing its impact as a risk assessment measure. Additionally, if the deficit proves to be even lower than what predicted, the control can find itself unprepared to face a scenario that's even less convenient than the one already assumed to be the worse. As a result, a sub-optimal (yet feasible) operation will take place. The predictive control will correct the errors, but on the long term this will result in additional costs taken in charge by the system.

A detailed analysis of the results for Fig. 4.9 confirms that the adoption of a worst-case scenario introduces losses from shedding and increases curtailment. An MPC with a median PV profile will instead reduce the load shedding to zero and decrease curtailment significantly, proving that a predictive logic is capable of efficiently correcting forecast errors, and a risk-averse control can be too conservative.

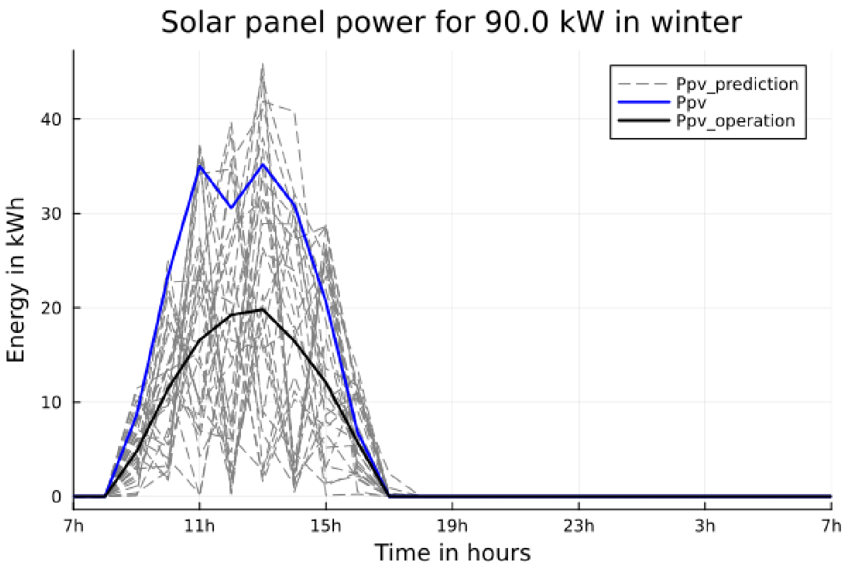

Figure 5.6: Stochastic PV profile for a configuration with 90 kWp of PV installed. The blue line represents the real generation, the black line the worst scenario among all the ones considered in the optimization, marked with gray dashed lines.

5.3.2. Effect of seasonal variation on configuration performance

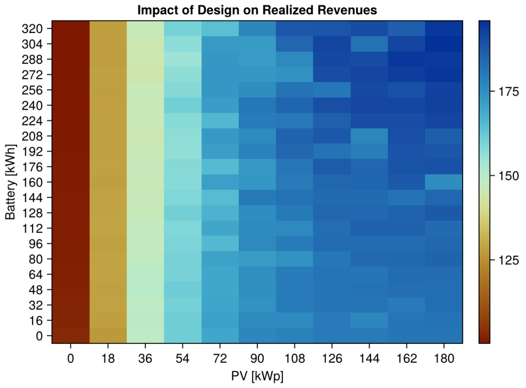

(a) Operation revenues in summer.

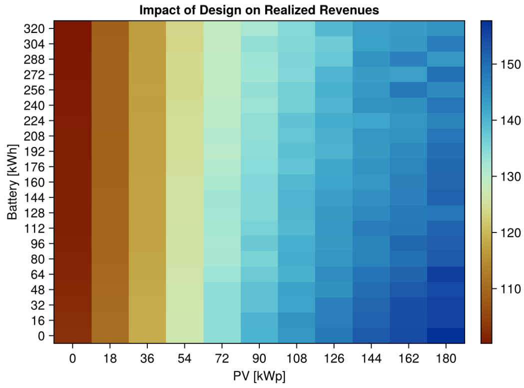

(b) Operation revenues in winter

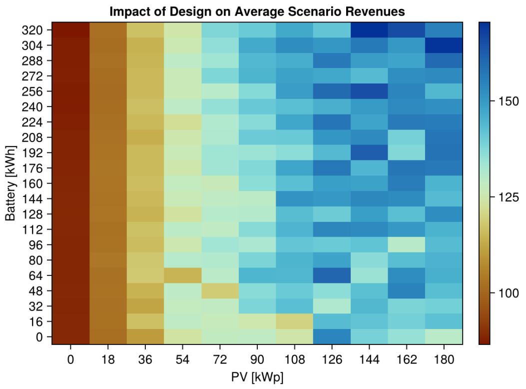

(c) Average revenues in summer.

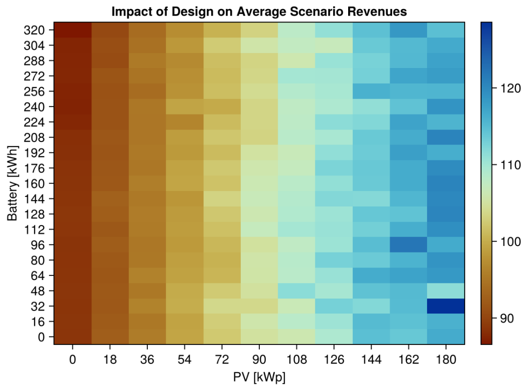

(d) Average revenues in winter.

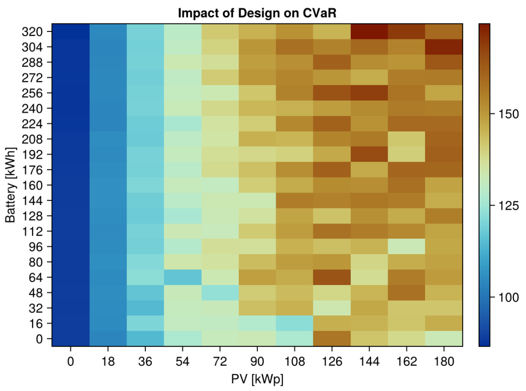

(e) Expected losses in summer.

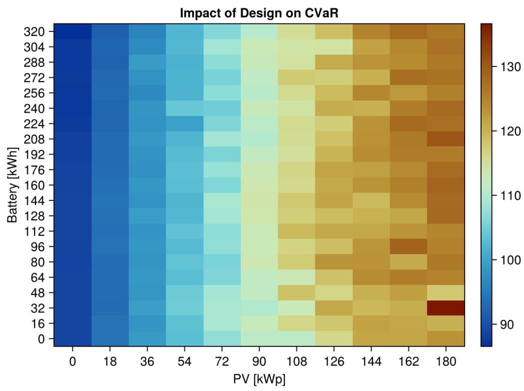

(f) Expected losses in winter.

Figure 5.7: Operation revenues, average scenario costs and CVaR values for reference days in summer and in winter changing the design parameters.

The optimal size of each component will be influenced by the availability of solar power in different seasonal periods. To visualize the revenues generated and the potential losses deriving from uncertainties, an analysis on a reference day in summer and in winter with a stochastic MPC at fixed parameters ($\lambda = 0.1, \epsilon = 0.8$) was performed for every configuration. The results are gathered in Fig. 5.7 : Fig. 5.7a and Fig. 5.7b show that the daily revenues generated in both seasons increase with the size of the solar panels, while the battery capacity has a different optimal value, being the maximum in summer and zero in winter. This highlights that the battery is a valuable asset when there is abundance of solar power available for storage, provided that the PV installed is high enough.
From a long-term perspective, this revenues should compensate the costs of installation of the components. Moreover, with more PV panels installed, the control will have to deal with uncertainties of higher magnitude, making the system more fragile and exposed to losses caused by reliance on unpredictable energy. This is reflected by the increasing value of the CVaR function in Fig. 5.7e and Fig. 5.7f for higher values of PV. Overall, changing the battery capacity does not produce a great change in revenues or losses, especially when reducing the capacity to zero. This means that the grid efficiently covers the system with a predictive control strategy, mitigating the risk resulting from unpredicted low solar irradiance, which in turn results in a moderate decrease in revenues. Risk assessment is therefore suitable for more extreme scenarios, where the expected losses from the realization of bad scenarios could be more relevant than the ones faced by this system.

5.3.3. Tuning of the risk aversion parameter

The effect of the CVaR function can be quantified by running the same analysis and change the λ parameter, evaluating the daily revenues with respect to the expected losses at different battery sizes. From the results in Fig. 5.7, a PV size of 180 kWp was chosen to guarantee enough energy availability to the battery. Results in Fig. 5.8 show that under a risk neutral condition the CVaR increases significantly, meaning that the tail of the cost distribution will be larger. Further increasing lambda make the frontier collapse on a fixed value of expected losses, demonstrating the effect of the CVaR in reducing the probability of dealing with scenarios with higher costs of operation.
Once again, the role of the battery changes seasonally, increasing profits in summer and decreasing them in winter. Additionally, without the correction of the CVaR function ($\lambda = 0$) the battery reduces expected losses in winter, proving to be a useful asset for energy availability in energy deficit situations, and turn into a speculative asset in summer, increasing profits and risk as well. This suggests that without risk assessment measures, a predictive control efficiently utilizes the battery in an effective way depending on the

availability of solar power.
Overall, increasing the battery capacity and considering risk can be a redundant increase in system complexity and safety measures, since a predictive control that is sufficiently covered by the grid can provide the operational flexibility needed to ensure an optimal performance in the long-term framework.

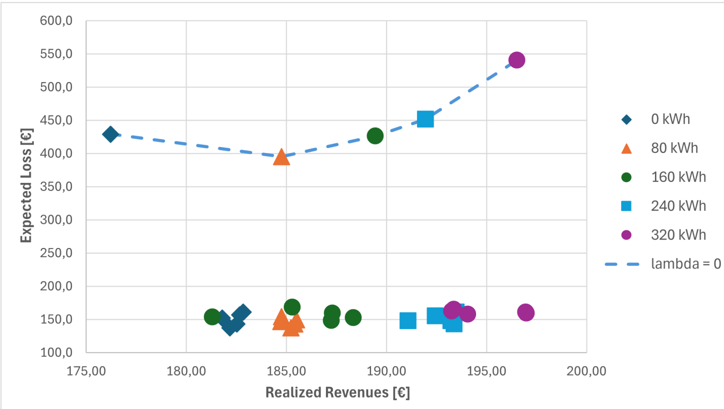

(a) Effect of λ on different configurations for a summer reference day.

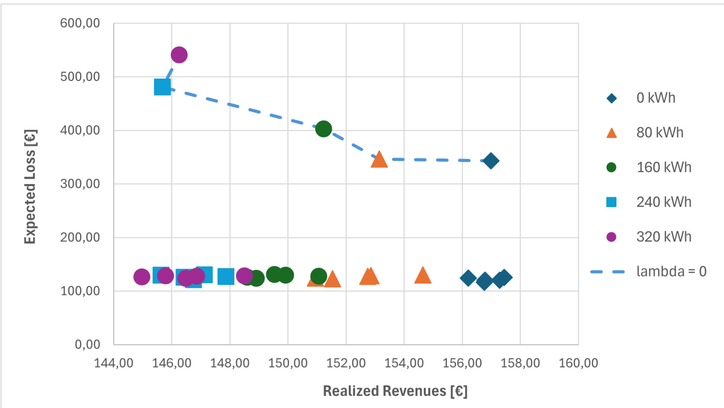

(b) Effect of λ on different configurations for a winter reference day.

Figure 5.8: Frontiers of expected losses versus realized revenues for reference days in summer and winter for different values of the risk aversion parameter λ. Each configuration has 180 kWp installed and every group of points is divided by battery capacity.

6 | Conclusions and Future Developments

A predictive control framework was embedded in a lifetime simulation searching for the optimal design of a green microgrid. Uncertainties on photovoltaic production and a risk measure were introduced to approximate realistic operation.
Results showed that the adopted control strategy influences the optimal long-term design. The system is sufficiently secure, since the battery can be substituted by the grid, and predictive control provides enough flexibility. Storage value was found to change seasonally, depending on the availability of photovoltaic energy. It will instead emerge in specific conditions dictated by the nature of the model: without a predictive logic in fact, the need for flexibility will be shifted to the system architecture.
A predictive logic effectively compensate forecast errors. A risk-aware formulation indicates that a more conservative model introduces unnecessary economic penalties, as uncertainty is already accounted for during online operation. This supports the use of MPC optimization for long-term economic planning.
Overall, predictive control significantly affects the long-term optimal design. Moreover, a flexible operation can outperform structural reinforcement with a simpler microgrid structure: even when exposed to uncertainties, smart-charging reaches satisfactory performance without increasing the system complexity. As a result, operational flexibility can substitute structural flexibility.

6.1. Limitations

The main limitation of this work lies in the computational burden of the predictive control optimization, which limited the representation of the system behavior in the configuration search space. However, this does not affect the qualitative conclusions, since the objective of the study was to assess the structural role of predictive control rather than to obtain specific design values.
Moreover, several assumptions were introduced to keep the optimization inside a well-

defined framework. While the representation of real energy management and economic planning is simplified, this allowed to isolate the interaction between predictive control, uncertainty, and system design, which represents the focus of this study.

6.2. Future Developments

Modeling of uncertainty can be extended also to loads and grid availability, where the effect of risk-aware optimization could be expected to play a more relevant role. Furthermore, the framework could be formulated as a multi-objective optimization including emissions, to better evaluate system sustainability. These extensions would allow to assess the proposed approach in less secure systems and support more extensive planning criteria for more realistic solutions.

Bibliography

[1] S. Ahmad, J. Baltussen, P. Kergus, Z. Kader, and S. Caux. A two-layers predictive algorithm for workplace ev charging. *IECON 2023 - 49th Annual Conference of the IEEE Industrial Electronics Society*, 2023.

[2] E. Antunes, B. Sareni, and X. Roboam. Optimal techno-economic and environmental design of a renewable energy based charging station including second life batteries. *The 26th European Conference on Power Electronics and Applications, GDR SEEDS France & EPE Association, Mar 2025, Paris, France*, 2025.

[3] C. Cortes-Aguirre, Y.-A. Chen, A. Ghosh, J. Kleissl, and A. Khurram. Economic mpc with an online reference trajectory for battery scheduling considering demand charge management. *IEEE Transactions on Smart Grid*, 16(6):4983–4996, 2025. doi: 10.1109/TSG.2025.3600047.

[4] J. Hu, Y. Shan, Y. Yang, A. Parisio, Y. Li, N. Amjady, S. Islam, K. W. Cheng, J. M. Guerrero, and J. Rodríguez. Economic model predictive control for microgrid optimization: A review. *IEEE Transactions on Smart Grid*, 15(1):472–484, 2024. doi: 10.1109/TSG.2023.3266253.

[5] M. T. Hussain, D. N. B. Sulaiman, M. S. Hussain, and M. Jabir. Optimal management strategies to solve issues of grid having electric vehicles (ev): A review. *Journal of Energy Storage*, 33:102114, 2021. ISSN 2352-152X.

[6] G. M. S. Kumar, X. Guo, S. Zhou, H. Luo, Q. Wu, Y. Liu, Z. Dou, K. Pan, Y. Xu, H. Yang, and S. Cao. State-of-the-art review of smart energy management systems for supporting zero-emission electric vehicles with x2v and v2x interactions. *Renewable and Sustainable Energy Reviews*, 208:115050, 2025. ISSN 1364-0321.

[7] R. Pitanga. Energy management of an ev charging station with a solar panel and a battery. Technical report, LAPLACE, 28 january 2025.

[8] R. T. Rockafellar and S. Uryasev. Optimization of conditional value-at risk. *Journal of Risk*, 3:21–41, 2000. URL `https://api.semanticscholar.org/CorpusID:854622`.

[9] Z. M. Salameh, B. S. Borowy, and A. Amin. Photovoltaic module-site matching based on the capacity factors. *IEEE Transactions on Energy Conversion*, 10:326–332, 1995. URL `https://api.semanticscholar.org/CorpusID:111146196`.

[10] R. V. X. d. Souza and T. Sousa. Analysis of demand response in electric systems with strong presence of intermittent generation using conditional value-at-risk. *Energies*, 17(18), 2024. ISSN 1996-1073. doi: 10.3390/en17184688. URL `https://www.mdpi.com/1996-1073/17/18/4688`.

[11] F. Wieberneit, E. Crisostomi, and R. Shorten. Effect of battery size on emission reduction of predictive electric vehicle charging control. pages 1–5, 2025.

[12] R. Wunderling. Advanced gurobi algorithms. *Gurobi Days Paris*, 2022. URL `https://www.gurobi.com/wp-content/uploads/2022-10-Paris_Advanced_Algorithms.pdf?x47079`.

[13] M. Yaseen, I. Fareed Nizami, M. B. Aldajani, A. Ali Raja, F. Haroon, and Q. Abbas. Resilient constraint energy management for microgrids: Integrating wasserstein dro and cvar-constrained mpc under renewable uncertainty. *IEEE Access*, 14:11534–11559, 2026. doi: 10.1109/ACCESS.2025.3648135.

[14] Z. Zhao, J. Guo, X. Luo, C. S. Lai, P. Yang, L. L. Lai, P. Li, J. Guerrero, and M. Shahidehpour. Distributed robust model predictive control-based energy management strategy for islanded multi-microgrids considering uncertainty. *IEEE Transactions on Smart Grid*, pages 1–1, 01 2022. doi: 10.1109/TSG.2022.3147370.

A | Appendix A: Optimization Models.

A.1. Structure of the MPC optimization problem

The decision variables of the MPC optimization problem are the overall power to the charging stations, the power exchanged with the battery, the predicted photovoltaic power and the energy in the battery, which form the decision vector (A.1):

$$x(t) = \begin{pmatrix} P_{EV}(t) \\ \vdots \\ P_{EV}(t_f) \\ P_{bat}(t) \\ \vdots \\ P_{bat}(t_f) \\ P_{PV}(t) \\ \vdots \\ P_{PV}(t_f) \\ \mathcal{W}(t+1) \\ \vdots \\ \mathcal{W}(t_f+1) \end{pmatrix} \in \mathbb{R}^{4n(t)}. \tag{A.1}$$

The upper and lower bound of the decision variables are defined, according to [7], as vectors containing their corresponding maximum and minimum values, defined as parameters of the system:

$$ub = \begin{pmatrix} P_{EV,max}\,\mathbf{1}_{n(t)\times 1} \\ P_{bat,max}\,\mathbf{1}_{n(t)\times 1} \\ Inf\mathbf{1}_{n(t)\times 1} \\ \mathcal{W}_{max}(t+1) \\ \vdots \\ \mathcal{W}_{max}(t_f+1) \end{pmatrix} \tag{A.2a}$$

$$lb = \begin{pmatrix} \mathbf{0}_{n(t)\times 1} \\ -P_{bat,max}\,\mathbf{1}_{n(t)\times 1} \\ \mathbf{0}_{n(t)\times 1} \\ \mathcal{W}_{min}(t+1) \\ \vdots \\ \mathcal{W}_{min}(t_f+1) \end{pmatrix} \tag{A.2b}$$

The objective is to minimize the intake from the grid, which corresponds to maximize the use of the renewable energy available, the objective function is written in this form:

$$\min \sum_{t=1}^{t_f} P_g(t) \tag{A.3}$$

Considering the definition of the objective function and also the power balance of the system solved for $P_g(t)$, by following the convention declared before:

$$\sum_{n=1}^{N} P_g(n) = f(n)^N x(n) \tag{A.4}$$

and:

$$P_g(t) = P_{EV}(t) - P_{bat}(t) - \hat{P}_{PV}(t) + P_r, \quad t = 1, 2, \dots, t_f. \tag{A.5}$$

we obtain the objective function as:

$$f(t) := \big(\underbrace{1, \dots, 1}_{n(t)\ \text{times}}, \underbrace{-1, \dots, -1}_{n(t)\ \text{times}}, \underbrace{-1, \dots, -1}_{n(t)\ \text{times}}, \underbrace{0, \dots, 0}_{n(t)\ \text{times}}\big)^T, \quad t = 1, 2, \dots, t_f. \tag{A.6}$$

The inequality constraints that take part in the formulation of the linear problem are described in the following. There are four groups of constraints, each one expressing a different feature of the system that the controller has to consider with a predictive logic throughout the time horizon. The first two groups of constraints represent the maximum and the minimum boundaries of the energy allocated to the charging station to recharge the buses. They are constructed in such a way that the cumulative amount of energy used for the recharge is considered as a state variable: in this way, the controller adapts to the current condition of the system. The first group deals with the upper bound:

$$\begin{cases} P^*_{EV,t} \cdot \Delta t \leq E^{max}_{t+1} - E_{EV,t} \\ P^*_{EV,t} \cdot \Delta t + P^*_{EV,t+1} \cdot \Delta t \leq E^{max}_{t+2} - E_{EV,t} \\ \vdots \\ P^*_{EV,t} \cdot \Delta t + P^*_{EV,t+1} \cdot \Delta t + \cdots + P^*_{EV,t_f-1} \cdot \Delta t \leq E^{max}_{t_f} - E_{EV,t} \end{cases} \tag{A.7}$$

The second group is in the same form and considers the lower bound:

$$\begin{cases} -P^*_{EV,t} \cdot \Delta t \leq E_{EV,t} - E^{min}_{t+1} \\ -P^*_{EV,t} \cdot \Delta t - P^*_{EV,t+1} \cdot \Delta t \leq E_{EV,t} - E^{min}_{t+2} \\ \vdots \\ -P^*_{EV,t} \cdot \Delta t - P^*_{EV,t+1} \cdot \Delta t - \cdots - P^*_{EV,t_f-1} \cdot \Delta t \leq E_{EV,t} - E^{min}_{t_f} \end{cases} \tag{A.8}$$

where values with an (*) are the decision variables of the controller that will have to be modified accordingly to the actual requirements of the system. As it is possible to see in (A.7), the amount of power that can be given to the charging stations must be below the corresponding amount of energy that would overcome the limit defined before. This is done by considering the time step chosen, the cumulative amount of energy that was given to the buses, $E_{EV,t}$, and its maximum value allowed *at the next time step*. This reasoning is the same for every remaining time step, such that all the future values of $P^*_{EV,t}$ are constrained. It is important to note that this system of constraints, as well as all the others, is valid from the present time step considered to the last one. The algorithm is in fact a "shrinking time horizon" model, as it solves a problem that gradually reduces its dimensions over time (precisely, at every time step). As it will be discussed in the following sections, this feature will impact on its performance (for example, when dealing with uncertainties), making it a reasonable choice with respect to other forms of predictive control. The third and fourth groups are formulated in a similar way and express the limits on the power that is taken or injected to the grid, recalling the power balance stated in

(A.5):

$$\begin{cases} P^*_{EV,t} - P^*_{batt,t} - P^*_{PV,t} \leq P_{grid,max} - P_r \\ P^*_{EV,t+1} - P^*_{batt,t+1} - P^*_{PV,t+1} \leq P_{grid,max} - P_r \\ \vdots \\ P^*_{EV,t_f-1} - P^*_{batt,t_f-1} - P^*_{PV,t_f-1} \leq P_{grid,max} - P_r \end{cases} \tag{A.9}$$

for the power that is taken from the grid, while for the power that is injected:

$$\begin{cases} -P^*_{EV,t} + P^*_{batt,t} + P^*_{PV,t} \leq P_{grid,max} + P_r \\ -P^*_{EV,t+1} + P^*_{batt,t+1} + P^*_{PV,t+1} \leq P_{grid,max} + P_r \\ \vdots \\ -P^*_{EV,t_f-1} + P^*_{batt,t_f-1} + P^*_{PV,t_f-1} \leq P_{grid,max} + P_r \end{cases} \tag{A.10}$$

Then the equality constraints are defined:

$$\begin{cases} P^*_{PV,t} = \hat{P}_{PV,t} \\ P^*_{PV,t+1} = \hat{P}_{PV,t+1} \\ \vdots \\ P^*_{PV,t_f-1} = \hat{P}_{PV,t_f-1} \end{cases} \tag{A.11}$$

In (A.11) all the variables related to the photovoltaic power are assigned with the predicted power at the corresponding time step. Finally,

$$\begin{cases} P^*_{batt,t} \cdot \Delta t + w_{t+1} = w_t \\ P^*_{batt,t+1} \cdot \Delta t - w_{t+1} + w_{t+2} = 0 \\ \vdots \\ P^*_{batt,t_f-2} \cdot \Delta t - w_{t_f-2} + w_{t_f-1} = 0 \\ w_{t_f} = w^* \end{cases} \tag{A.12}$$

the equation (A.12) defines the link between the energy inside the battery and the power that flows in and out accordingly to the convention used. The value of w^* is fixed at 50% of the battery capacity.

The power that is needed or given from the grid is described as:

$$P_{grid,t} = P_{EV,t} + P_r - P_{batt,t} - P_{PV,t} \tag{A.13}$$

Where $P_{grid,t}$ represents the value of energy needed from the grid as a result of the power balance in the system, and it is minimized by the objective function.

At the end of the simulation it is possible to define the following parameters to evaluate the performance of the system:

$$Satisfaction = 100 \cdot \frac{E_{EV,t_f}}{E_{EV,TOT}} \tag{A.14}$$

$$Selfconsumption = 100 \cdot \frac{(\sum_t^{t_f-1} P_{PV,t} - \sum_t P_{grid,out,t})}{\sum_t^{t_f-1} P_{PV,t}} \tag{A.15}$$

$$Selfproduction = 100 \cdot \frac{(\sum_t^{t_f-1} P_{PV,t} - \sum_t P_{grid,out,t})}{E_{EV,t_f-1} + E_r} \tag{A.16}$$

Equations (A.14), (A.15) and (A.16) show how much the controller is capable to satisfy the demand, while keeping a good degree of self-production and self-consumption. $E_{EV,TOT}$ was assumed as the sum of all the energy that has to be given to the buses, while E_r stands as the total energy of the auxiliaries that in the system is represented as a resistive charge.

This problem is solved with an interior point method, and the solution is taken as the optimal energy management of the system at the corresponding time step, considering the state of the system and the rest of the day.

A.2. Structure of the MILP optimization problem

The objective function of the MILP optimization problem is the following:

$$\begin{aligned} \min \sum_{t \in t} (C_{grid,in}(t) \cdot P_{grid,in}(t) - C_{grid,out} \cdot P_{grid,out}(t) \\ + C_{BT,E_{BT,exch}} \cdot (P_{BT,ch}(t) + P_{BT,dch}(t)) - C_{tariff,EV} \cdot (P_{CS}(t) - P_{shed}(t))) \cdot \Delta t \end{aligned} \tag{A.17}$$

From (A.17) we can point out two main differences regarding the formulation of this problem: first, the optimization is performed once for all the time horizon, instead of being solved multiple times to adapt to the actual state of the system. This decreases greatly the computational time with respect to the predictive algorithm. Also, the objective function itself now minimizes the costs of operation instead of the power taken from the grid. This introduces other assumptions, such as the electricity tariffs, that will behave as weights of the decision variables in the objective function. Their value was kept the same as reported in [2]. It is also important to note that the cost assumed for the exchange with the battery was assumed to be zero as it is internal to the system. The constraints were defined, as explained in [2], to respect the limits on the State of Charge (A.20), on the maximum power admissible exchanged with the grid (A.19), and the system's power balance (A.18) that are reported here for clarity:

$$P_{grid,in}(t) + P_{PV}(t) + P_{BT,dch}(t) + P_{shed}(t) = P_{CS}(t) + P_{BT,ch}(t) + P_{grid,out}(t) + P_{curt}(t) \tag{A.18}$$

The slack variables P^t_{curt} and P^t_{shed} visible in (A.17) and (A.18) are needed to represent the curtailment of the photovoltaic power and the shedding of the demand that could occur. This choice represents another difference with the previous model, which considers a prediction of the photovoltaic power and has a variable power profile to allocate to the buses, and therefore cannot consider curtailment and shedding variables directly inside the optimization problem, but rather has to adapt to them in the following iterations.

$$P_{grid,in}(t) \leq P_{grid,lim} \tag{A.19a}$$

$$P_{grid,out}(t) \leq P_{grid,lim} \tag{A.19b}$$

From (A.19) it is worth pointing out that for this problem, while the convention of signs remains the same, it was chosen to represent only positive variables for each power flowing in each direction, instead of having one variable that could assume both positive and negative values. Equations (A.20) and (A.21) represent the constraints on the state of charge (SoC) of the battery, where η_{BT} is the efficiency of the battery, which in the previous model is considered only after the optimization:

$$SoC(t+1) = SoC(t) - \left(\frac{P_{BT,dch}(t)}{\eta_{BT}} - P_{BT,ch}(t) \cdot \eta_{BT} \right) \cdot \frac{\Delta t}{E_{BT,tot}(t)} \tag{A.20}$$

$$SoC_{min} \leq SoC(t) \leq SoC_{max} \tag{A.21a}$$

$$SoC^0 = SoC^{ini} \tag{A.21b}$$

$$SoC^{end} \geq SoC^{ini} \tag{A.21c}$$

This is a Mixed Integer Linear Problem (MILP) solved for a week of operation with an hourly time step. There is no prediction on the photovoltaic production, so the model considers it as perfectly known. Likewise, the power to the EVs is already defined. The objective function considered this time involved the cost of the power taken from the grid, to be minimized. The battery state of health (SoH) is updated at the end of every simulated week, and the additional constraints on its remaining capacity are placed to verify if a replacement is needed. If this is the case, the installation of a new battery is considered, along with its costs and externalities. After the simulation on the whole lifetime takes place, the operation costs are actualized to each year and the values of the Net Present Cost along with the Global Warming Potential are calculated as described in [2]. With these two final values, a single configuration (in terms of battery capacity and photovoltaic peak power) is characterized. The screening will proceed to the next one and repeat the lifetime simulation. As it is possible to see from (A.17), the problem hereby considered is a single objective optimization based on the operation costs. This means that the generated emissions are not involved in the optimization, and the tradeoff between the Net Present Cost (NPC) and with the Global Warming Potential (GWP) can be discussed when finding a Pareto curve made of the non-dominated configurations that resulted from the screening.

A.3. Control logic of the lower layer in the MPC function

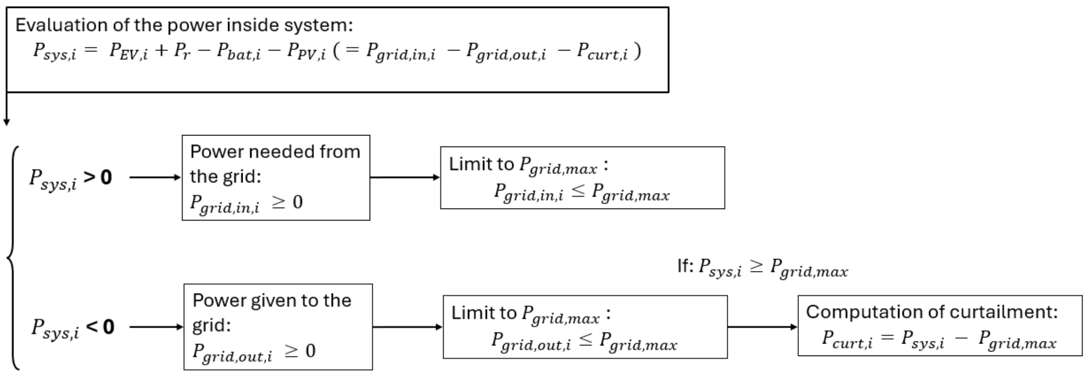

Figure A.1: Diagram of the control logic implemented in the MPC algorithm when considered inside the lifetime simulation algorithm.

A.4. Microgrid structure scheme

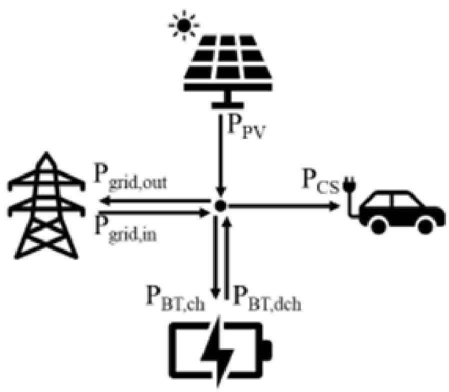

Figure A.2: Scheme of the microgrid structure. The directions in which the power can be exchanged are defined accordingly to the nature of the components.

B | Appendix B: Testing and Implementation

B.1. Impact of time step on MPC computational time and performance

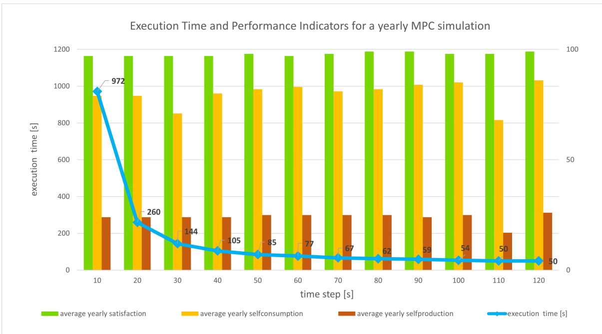

Figure B.1: This plot shows the decrease in the execution time of a one-year simulation when increasing the time step, along with the corresponding performance indicators. The desired time to simulate one year was around 60 seconds.

B.2. Comparison between Rolling and Shrinking time horizon MPC

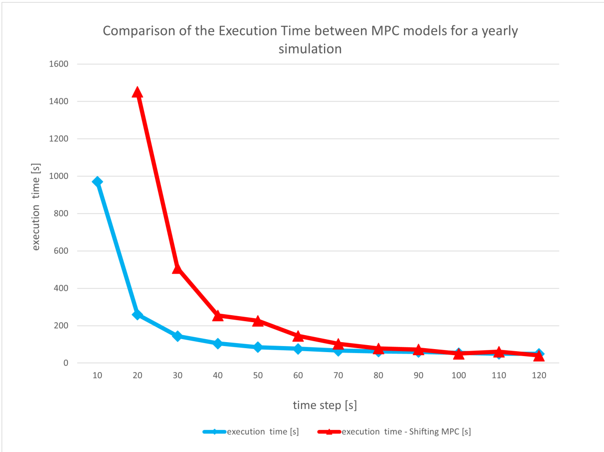

Figure B.2: Comparison of the simulation time for the two MPC models considered. Each point corresponds to a yearly simulation.

B.3. Solver Choice

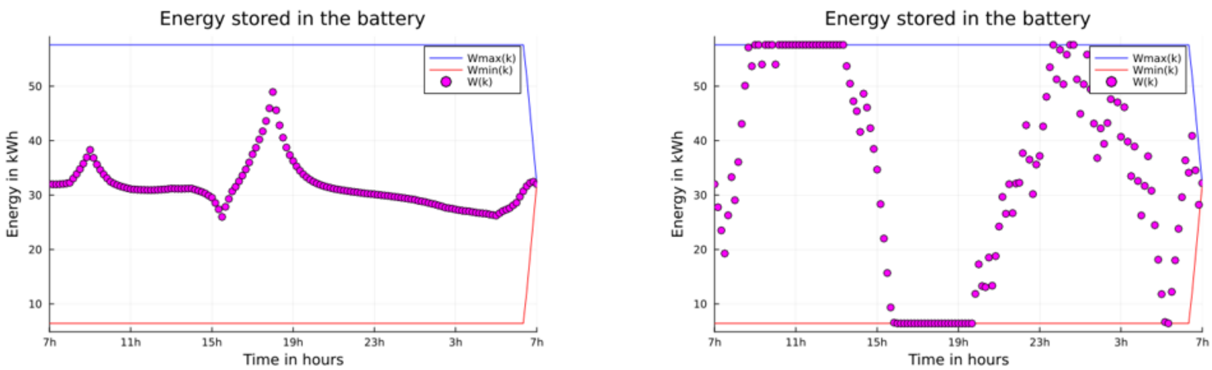

(a) Energy inside the battery using the HSD solver from Tulip. The trend is smooth, meaning that the power exchanged with the system doesn't have excessive instantaneous values.

(b) Energy inside using the Dual Simplex model from Gurobi. The unstable trend as well as the saturation at both charge limits results from frequent cycles at high power, an operation that induces stress in the battery.

Figure B.3: Comparison of the energy management inside the battery for a day of operation using different solvers. The HSD from Tulip was implemented.

C | Appendix C: Complementary Results

C.1. Position of Pareto Fronts in the design search space found using different models

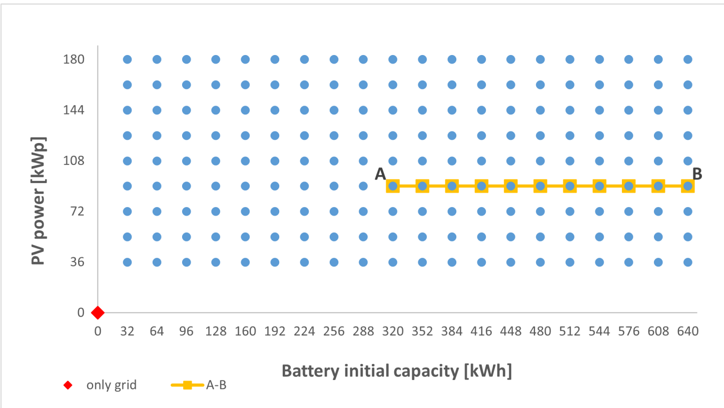

Figure C.1: The optimal design configurations found with a screening for an SLB case with a weekly time horizon MILP algorithm.

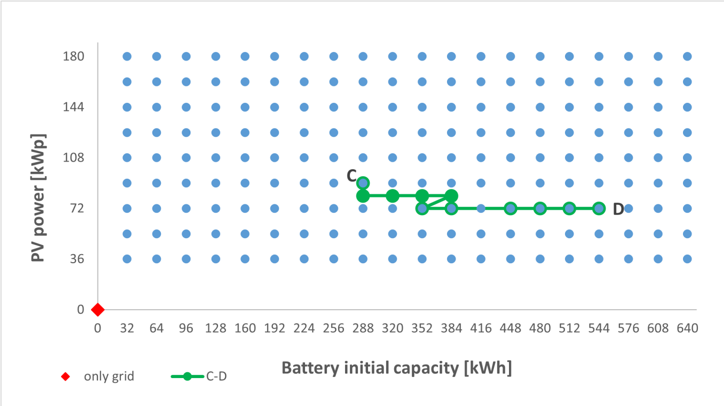

Figure C.2: The Pareto curve obtained with the 24-hours time horizon MILP model. It is still in the same area of the search space as the one obtained with the weekly time horizon MILP.

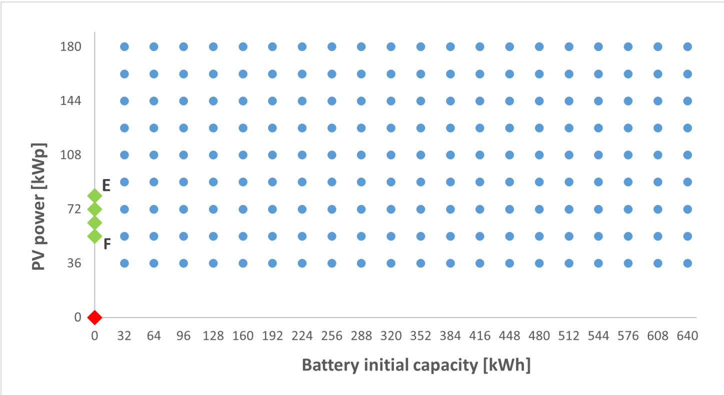

Figure C.3: Corresponding configurations found with a predictive control algorithm. The Pareto front involves no battery.

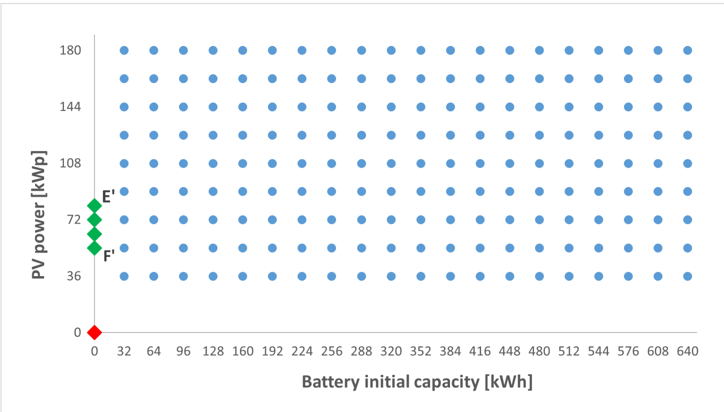

Figure C.4: The curve E'-F' in the search space of the screening carried out with an MPC model with a prediction on the PV power. This curve is equivalent to the points obtained before.

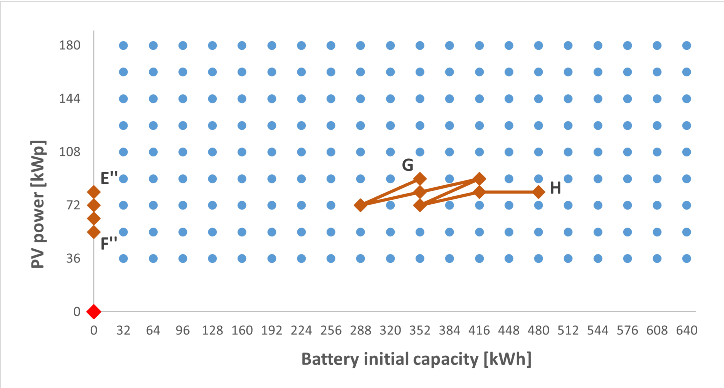

Figure C.5: Position of the Pareto Curve in the search space using an MPC model considering a constant lower bound on the battery energy.

List of Figures

Acknowledgments

This thesis is based on the work carried out on the I-REVE project by several professors, postdocs and researchers at the LAPLACE laboratory in Toulouse, France. I wish to express my gratitude to M. Xavier Roboam and to M. Bruno Sareni, and to Mme. Pauline Kergus and Mme. Evelise Antunes, who supervised my internship with great participation and included me without reserves in a new and stimulating environment.